Bioorganic Chemistry 108 (2021) 104665

Contents lists available at ScienceDirect

Bioorganic Chemistry

journal homepage: www.elsevier.com/locate/bioorg

Pyrazoline analogs as potential anticancer agents and their apoptosis, molecular docking, MD simulation, DNA binding and antioxidant studies

Manish Rana [a], Rizwan Arif [a], Faez Iqbal Khan [b], Vikas Maurya [c], Raja Singh [c], Md Imam Faizan [d], Shama Yasmeen [a], Sajad Hussain Dar [a], Raquib Alam [e], Ankita Sahu [f], Tanveer Ahmad [d], Rahisuddin [a,*]

[a] Department of Chemistry, Jamia Millia Islamia, New Delhi 110025, India
[b] School of Electronic Science and Engineering, University of Electronic Science and Technology of China, China
[c] Special Centre for Molecular Medicine, Jawharlal Nehru University, New Delhi 110067, India
[d] Multidisciplinary Centre for Advanced Research & Studies, Jamia Millia Islamia, New Delhi 110025, India
[e] Department of Applied Sciences, University Polytechnic, Jamia Millia Islamia, New Delhi 110025, India
[f] ICMR-National Institute of Pathology, Safdarjung Hospital Campus, New Delhi 110029, India

ARTICLE INFO

Keywords:
N-formyl pyrazoline
Anticancer
Ct-DNA
Antioxidant
Molecular modelling
MD simulations

ABSTRACT

N-formyl pyrazoline derivatives (**3a–3l**) were designed and synthesized via Michael addition reaction through cyclization of chalcones with hydrazine hydrate in presence of formic acid. The structural elucidation of *N*-formyl pyrazoline derivatives was carried out by various spectroscopic techniques such as ^{1}H, ^{13}C NMR, FT-IR, UV–visible spectroscopy, mass spectrometry and elemental analysis. Anticancer activity of the pyrazoline derivatives (**3a–3l**) was evaluated against human lung cancer (**A549),** fibrosarcoma cell lines (**HT1080)** and human primary normal lung cells (**HFL-1)** by MTT assay. The results of anticancer activity showed that potent analogs **3b** and **3d** exhibited promising activity against **A549** (IC_{50} = 12.47 ± 1.08 and 14.46 ± 2.76 μM) and **HT1080** (IC_{50} = 11.40 ± 0.66 and 23.74 ± 13.30 μM) but low toxic against the **HFL-1** (IC_{50} = 116.47 ± 43.38 and 152.36 ± 22.18 μM). The anticancer activity of potent derivatives (**3b** and **3d**) against A549 cancer cell line was further confirmed by flow cytometry based approach. DNA binding interactions of the pyrazoline derivatives **3b** and **3d** have been carried out with calf thymus DNA (Ct-DNA) using absorption, fluorescence and viscosity measurements, circular dichroism and cyclic voltammetry. Antioxidant potential of *N*-formyl pyrazoline derivatives (**3a–3l**) has been also estimated through DPPH (2,2-diphenyl-1-picrylhydrazyl) free radical and H_2O_2. Results revealed that all the compounds exhibited significant antioxidant activity. In silico molecular modelling and ADMET properties of pyrazoline derivatives were also studied using PyRx software against topoisomerase II receptor with PDB ID: 1ZXM to explore their best hits. MD simulation of 3b and 3d was also carried out with topoisomerase II for structure–function correlation in a protein. HuTopoII inhibitory activity of the analogs (3a–3l) was examined by relaxation assay at varying concentrations 100–1000 μM.

1. Introduction

Cancer is defined by a rapid, uncontrolled and pathological proliferation of the cells which is a second leading cause of deaths globally. Cancer is a group of diseases, spread almost all the body parts (organ or tissue) and develops after the body's control mechanism stops working and uncontrolled growth and division of cell takes place too quickly [1–4]. The heterocyclic analogs are universal in medicinal chemistry due to their unparallel intrinsic versatility [5–8]. Owing to their significant pharmaceutical properties, pyrazoline derivatives have received appreciable attention in various fields [9,10]. Pyrazolines have been proven as the most useful framework for diversified biological activities such as antibacterial [11,12] anticancer [13,14] antifungal [15], anti-inflammatory [16,17], anti-oxidant [18,19] and antimalarial [20,21]. Pyrazolines, are a class of electron-rich nitrogen heterocyclic compounds having versatility in the medicinal chemistry and are being reported to exhibit remarkable anticancer effects by inhibiting the enzymes which promote cell division [22]. DNA is the primary

* Corresponding author.
E-mail address: rahisuddin@jmi.ac.in (Rahisuddin).

https://doi.org/10.1016/j.bioorg.2021.104665
Received 16 September 2020; Received in revised form 8 December 2020; Accepted 16 January 2021
Available online 27 January 2021

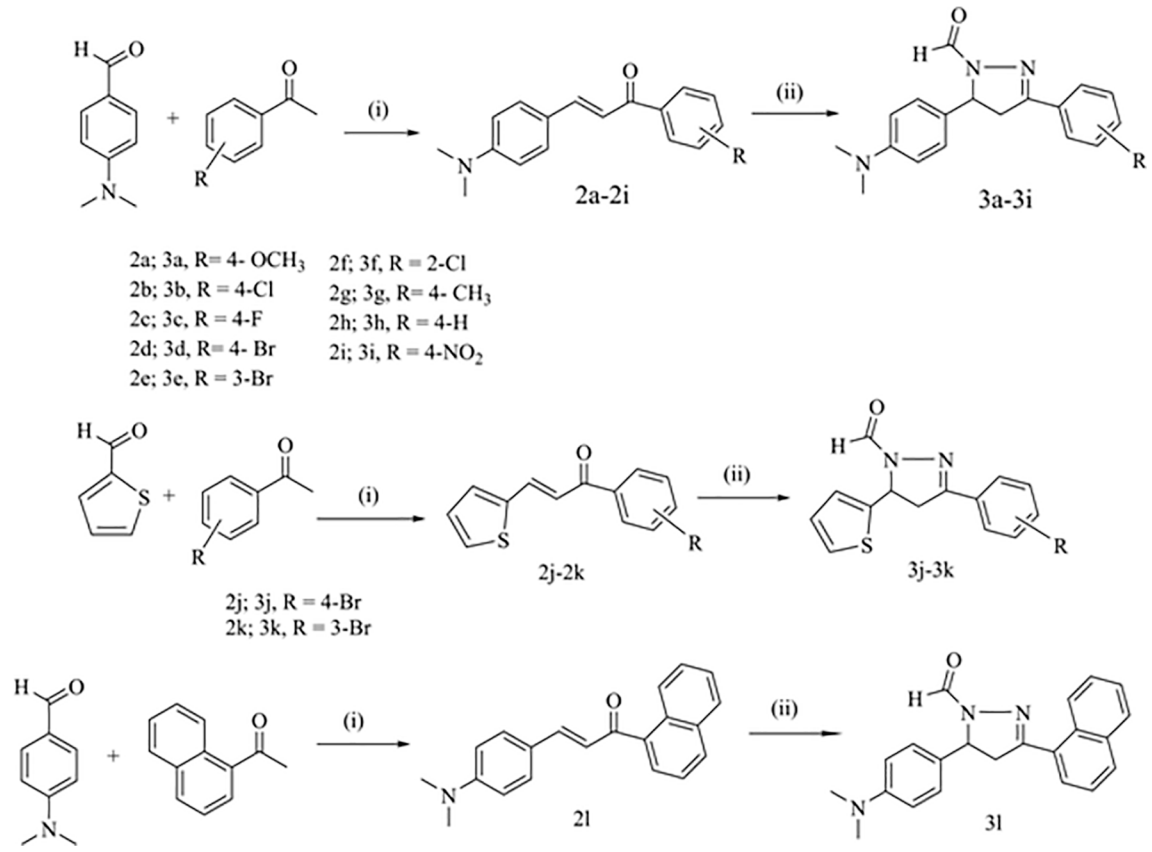

Scheme 1. General procedure for the synthesis of *N*-formyl pyrazoline derivatives (**3a–3l**). (i) NaOH (50%), absolute alcohol, room temperature, stir; (ii) $NH_2NH_2{\cdot}H_2O$/HCOOH, reflux for 4–6 h.

intracellular target for the anticancer drugs. In recent years, researchers have studied the interaction of drugs and DNA which may be responsible for the damage of DNA by preventing the quick division of cancer cells [23–26]. Drug or small molecules can interact with DNA through non-covalent, intercalation, groove binding or electrostatic binding mode [27,28]. Among these interactions, intercalation is one of the most significant DNA-binding mode, which is related to the antitumor activity of the compounds [29,30]. The rigidity induced by the incorporation of pyrazoline ring within the chalcone framework has earlier been proven to be extremely useful as far as cytotoxic potential is concerned [31–33]. Molecular docking and absorbed, distributed, metabolized and eliminated (ADMET) properties are widely employed to find out the novel hits for topoisomeraseII target [34,35].

Here, we aimed to design and synthesize a series of 3,5-diaryl-4,5-dihydropyrazoline derivatives with their anticancer activity against human lung cancer (A549), fibrosarcoma cell lines (HT1080) and human primary normal lung cells (HFL-1). The present research work involves the apoptosis evaluation, HuTopoII inhibitory activity, molecular docking, MD simulation, DNA-binding, antioxidant assay and ADMET properties of pyrazoline derivatives.

2. Experimental section

2.1. Materials and methods

All the reagents were commercially available and used as received without further purification. Acetophenones (Spectrochem), formic acid (Fisher scientific), hydrazine hydrate and substituted aldehydes (S.D. Fine Chemicals) were purchased. The elemental analysis of the *N*-formyl pyrazoline derivatives was ascertained by the Elementar CHNS analyzer. The melting points of the compounds were determined in open capillaries and are uncorrected. Reaction progress was routinely monitored by TLC (thin layer chromatography) using silica gel (precoated 60 F_{254}Al sheets, Merck). IR spectra of the synthesized compounds were recorded on Agilent Technologies and expressed in wavenumber (cm^{-1}). ^1H and ^{13}C NMR spectra were recorded using $CDCl_3$ as solvent on a Bruker 300 MHz spectrometer. Chemical shifts (δ) were given in ppm and tetramethylsilane (TMS) used as reference. To investigate the DNA-drug interaction, IVIUM potentiostat was used with a three-electrode system that was obtained from Metrohm, Dropsens (DS 220BT). Circular dichroism experiments were carried out by the Jasco J-815 spectrometer using a rectangular quartz cell of 1 cm path length. Fluorescence spectra were recorded at room temperature using an Agilent spectrophotometer. Electronic spectra of the compounds were obtained on a Labman UV–Visible spectrophotometer. Viscosity measurements were carried out using Ostwald viscometer at room temperature. The mass spectral analysis of the *N*-formyl pyrazoline derivatives was determined by LC MS/MS Waters.

2.2. General procedure for the synthesis of N-formyl pyrazoline derivatives (3a–3l)

The chalcone derivatives (**2a**–**2l**) were synthesized by condensation of aldehydes and substituted acetophenones in ethanol using sodium hydroxide as a base, according to the reported procedure [36]. To the chalcones **(2a–2l)**, 5.0 ml formic acid and hydrazine hydrate (0.5 ml, 10 mmol) were added dropwise and then the reaction mixture was refluxed for 4–6 h. The progress of the reaction was monitored by TLC (thin layer chromatography) in ethyl acetate and hexane (1:3) as effluent. After the completion of reaction, the warm reaction mixture was poured into ice-cold water and neutralized by a 1 M NaOH solution. The precipitate was filtered off, washed with cold water and dried in vacuum desiccator over

fused $CaCl_2$ and recrystallized in chloroform affording pyrazoline derivatives (**3a–3l**). The synthesis of pyrazoline derivatives is shown in Scheme 1.

*2.2.1. 5-(4-(dimethylamino)phenyl)-3-(4-methoxyphenyl)-4,5-dihydro-1H-pyrazole-1-carbaldehyde **(3a)***

Light green, Yield 80%. Mp: 130 °C. IR (neat, ν_{max} cm^{-1}): ν(C═O) 1611, ν(C═N) 1562. ^1H NMR ($CDCl_3$, 300 MHz ppm): 7.67–7.69 (d, 2H), 7.11–7.26 (d, 2H), 6.93–6.95 (d, 2H), 6.66–6.69 (d, 2H), 8.91 (s, 1H), 5.43 (dd, J = 4.6 and 17.8 Hz, 1H), 3.72 (dd, J = 11.8 and 17.7 Hz, 1H), 3.19 (dd, J = 4.6 and 11.8 Hz, 1H), 2.95 (s, 6H), 3.85 (s, 3H).^{13}C NMR ($CDCl_3$, 75.47 MHz): 161.48, 159.89, 155.64, 150.26, 129.02, 128.51, 128.29, 126.75, 123.79, 144.21, 112.75, 58.56, 55.43, 42.58, 40.55.MS (*m/z*): 324.20 (M + 1), Calculated %: $C_{19}H_{21}N_3O_2$: C 70.57; H 6.55; N 12.99. Found, %: C 70.56; H 6.57; N 12.95.

*2.2.2. 3-(4-chlorophenyl)-5-(4-(dimethylamino)phenyl)-4,5-dihydro-1H-pyrazole-1-carbaldehyde **(3b)***

Green, Yield 75%. Mp: 180 °C. IR (neat, ν_{max} cm^{-1}): ν(C═O) 1615, ν(C═N) 1523. ($CDCl_3$, 300 MHz ppm): 7.66–7.69 (d, 2H), 7.39–7.42 (d, 2H), 7.11– 7.26(d, 2H), 6.66–6.69(d, 2H), 8.92 (s, 1H),5.46 (dd, J = 4.5 and 11.6 Hz, 1H), 3.71 (dd, J = 11.8 and 17.7 Hz, 1H), 3.18 (dd, J = 5.1 and 17.7 Hz, 1H), 2.90 (s, 6H).^{13}C NMR ($CDCl_3$, 75.47 MHz): 160.07, 154.69, 150.32, 136.49, 129.70, 129.08, 128.53, 128.11, 126.73, 112.72, 58.89, 42.38, 40.51.MS (*m/z*): 328.17 (M + 1), Calculated %: $C_{18}H_{18}ClN_3O$: C 65.95; H 5.53; N 12.82. Found, %: C 65.95; H 5.48; N 12.85.

*2.2.3. 5-(4-(dimethylamino)phenyl)-3-(4-fluorophenyl)-4,5-dihydro-1H-pyrazole-1-carbaldehyde **(3c)***

Light green, Yield 82%. Mp: 148 °C. IR (neat, ν_{max} cm^{-1}): ν(C═O) 1579, ν(C═N) 1497. ^1H NMR (300 MHz, $CDCl_3$) δ 7.65–7.68 (d, 4H), 7.37–7.40 (d, 2H), 7.09–7.12 (d, 2H), 6.65–6.68, (d, 2H), 8.92 (s, 1H), 5.45 (dd, *J* = 17.8, 4.1 Hz, 1H), 3.71 (dd, *J* = 17.7, 11.7 Hz, 1H), 3.16 (dd, *J* = 11.7, 4.2 Hz, 1H), 2.93 (s, 6H). ^{13}C NMR (75 MHz, $CDCl_3$) δ 160.07, 154.69 150.31, 136.47, 129.70, 129.08, 128.54, 128.12, 127.91, 127.25, 126.73 112.71, 58.89, 42.38, 40.52.MS (*m/z*): 312.28 (M + 1), Calculated, %: $C_{18}H_{18}FN_3O$: C 69.44; H 5.83; N 13.50. Found, %: C 69.47; H 5.84; N 13.51.

*2.2.4. 3-(4-bromophenyl)-5-(4-(dimethylamino)phenyl)-4,5-dihydro-1H-pyrazole-1-carbaldehyde **(3d)***

White, Yield 75%. Mp: 170 °C. IR (neat, ν_{max} cm^{-1}): ν(C═O) 1658, ν(C═N) 1591. ^1H NMR ($CDCl_3$, 300 MHz): 7.65–7.68 (d, 2H), 7.38–7.41 (d, 2H), 7.10– 7.13 (d, 2H), 5.45 (dd, J = 4.5 and 17.7 Hz, 1H), 3.71 (dd, J = 11.8 and 17.7 Hz, 1H), 3.18 (dd, J = 4.5 and 11.8 Hz, 1H), 2.49 (s, 6H). ^{13}C NMR ($CDCl_3$, 75.47 MHz): 159.83, 151.46, 150.32, 134.65, 132.97, 132.00, 129.06, 128.96, 128.07, 127.70, 127.28, 126.75, 112.72, 58.81, 43.16, 40.53. MS (*m/z*): 372.13 (M + 1), Calculated %: $C_{18}H_{18}BrN_3O$: C 58.08; H 4.87; N 11.29 Found %: C 65.95; H 5.48; N 12.85.

*2.2.5. 3-(3-bromophenyl)-5-(4-(dimethylamino)phenyl)-4,5-dihydro-1H-pyrazole-1-carbaldehyde **(3e)***

Light green, Yield 78%. Mp: 200 °C. IR (neat, ν_{max} cm^{-1}): ν(C═O) 1600, ν(C═N) 1460. ^1H NMR (300 MHz, $CDCl_3$) 7.57–7.69 (m, 4H), 7.10–7.12 (d, 2H), 6.65–6.68 (d, 2H), δ 8.92 (s, 1H), 5.46 (dd, *J* = 17.6, 4.6 Hz, 1H), 3.72 (dd, *J* = 17.8, 11.7 Hz, 1H), 3.18 (dd, *J* = 11.8, 4.8 Hz, 1H), 2.91 (s, 6H).^{13}C NMR ($CDCl_3$, 75.47 MHz): 160.06, 154.72, 150.33, 132.03, 132.01, 130.00, 128.09, 128.07, 126.72, 124.84, 123.01, 112.71,58.90, 42.32, 40.51.MS (*m/z*): 372.20 (M + 1), Calculated %: $C_{18}H_{18}BrN_3O$: C 58.08; H 4.87; N 11.29. Found %: C 58.11; H 4.85; N 11.31.

*2.2.6. 3-(2-chlorophenyl)-5-(4-(dimethylamino)phenyl)-4,5-dihydro-1H-pyrazole-1-carbaldehyde **(3f)***

Yellow, Yield 70%. Mp: 195 °C. IR (neat, ν_{max} cm^{-1}): ν(C═O) 1579, ν(C═N) 1477. ($CDCl_3$, 300 MHz ppm): 7.78–7.90 (d, 2H), 7.66–7.69 (d, 2H), 7.11–7.26(m, 3H), 6.65–6.69 (d, 2H), 8.93 (s, 1H), 5.48 (dd, J = 4.5 and 17.7 Hz, 1H), 3.73 (dd, J = 11.5 and 17.7 Hz, 1H), 3.19 (dd, J = 4.5 and 11.7 Hz, 1H), 2.94 (s, 6H).^{13}C NMR ($CDCl_3$, 75.47 MHz): 160.07, 154.70, 150.30, 136.49, 129.66, 129.08, 128.09, 127.90, 126.72, 112.70, 58.88, 42.39, 40.53.MS (*m/z*): 328.23(M + 1), Calculated %: $C_{18}H_{18}ClN_3O$: C 65.95; H 5.53; N 12.82. Found, %: C 65.94; H 5.55; N 12.80.

*2.2.7. 5-(4-(dimethylamino)phenyl)-3-(p-tolyl)-4,5-dihydro-1H-pyrazole-1-carbaldehyde **(3g)***

Light green, Yield 72%. Mp: 140 °C. IR (neat, ν_{max} cm^{-1}): ν(C═O) 1588, ν(C═N) 1460. ^1H NMR (300 MHz, $CDCl_3$) δ 7.62–7.65 (d, 2H), 7.22–7.26 (d, 2H), 7.12–7.14 (d, 2H), 6.66–6.68 (d, 2H), 8.92 (s, 1H), 5.45 (dd, *J* = 17.6, 4.6 Hz, 1H), 3.74 (dd, *J* = 17.8, 11.7 Hz, 1H), 3.21 (dd, *J* = 11.8, 4.8 Hz, 1H), 2.93 (s, 6H), 2.40 (s, 3H). ^{13}C NMR ($CDCl_3$, 75.47 MHz): 160.01, 155.98, 150.26, 140.91, 129.51, 128.46, 128.37, 130.00, 126.76, 126.64, 112.74, 58.61, 42.53, 40.55, 21.53.MS (*m/z*): 308.21 (M + 1) Calculated %: $C_{19}H_{21}N_3O$: C 74.24; H 6.89; N 13.67. Found, %: C 74.29; H 6.92; N 13.68.

*2.2.8. 5-(4-(dimethylamino)phenyl)-3-phenyl-4,5-dihydro-1H-pyrazole-1-carbaldehyde **(3h)***

Light green, Yield 68%. Mp: 135 °C. IR (neat, ν_{max} cm^{-1}): ν(C═O) 1615, ν(C═N) 1560. ^1H NMR (300 MHz, $CDCl_3$) δ 7.73–7.76 (d, 2H), 7.43 – 7.45 (d, 2H), 7.12–7.15 (d, 2H), 6.66–6.69 (d, 2H), 8.94 (s, 1H), 5.47 (dd, *J* = 17.6, 4.6 Hz, 1H), 3.76 (dd, *J* = 17.8, 11.7 Hz, 1H), 3.23 (dd, *J* = 11.8, 4.8 Hz, 1H), 2.92 (s, 6H).^{13}C NMR ($CDCl_3$, 75.47 MHz): 160.10, 155.88, 150.29, 131.16, 130.52, 128.80, 128.55, 128.35, 126.76, 126.67, 112.74,58.72, 42.48, 42.54. MS (*m/z*): 294.18 (M + 1), Calculated %: $C_{18}H_{19}N_3O$: C 73.69; H 6.53; N 14.32. Found, %: C 73.70; H 6.48; N 14.34.

*2.2.9. 5-(4-(dimethylamino)phenyl)-3-(4-nitrophenyl)-4,5-dihydro-1H-pyrazole-1-carbaldehyde **(3i)***

Yellow, Yield 86%. Mp: 175 °C. IR (neat, ν_{max} cm^{-1}): ν(C═O) 1590, ν(C═N) 1460. ^1H NMR (300 MHz, $CDCl_3$) δ 8.27–8.30 (d, 2H), 7.88–7.91 (d, 2H), 7.10–7.13 (d, 2H), 6.66–6.69 (d, 2H), 8.96 (s, 1H), 5.52 (dd, *J* = 17.8, *J* = 4.9 Hz, 1H), 3.79 (dd, *J* = 17.8, 11.6 Hz, 1H), 3.26 (dd, *J* = 11.7, 4.9 Hz, 1H), 2.95 (s, 6H).^{13}C NMR ($CDCl_3$, 75.47 MHz): 160.44, 159.49, 154.91, 150.38, 148.51, 137.49, 128.91, 128.26, 127.14, 124.45, 112.86, 59.27, 56.47, 42.42. MS (*m/z*): 339.19(M + 1), Calculated %: $C_{18}H_{18}N_4O_3$: C 63.89; H 5.36; N 16.56. Found, %: C 63.85; H 5.41; N 16.58.

*2.2.10. 3-(4-bromophenyl)-5-(thiophen-2-yl)-4,5-dihydro-1H-pyrazole-1-carbaldehyde **(3j)***

White, Yield 77%. Mp: 145 °C. IR (neat, ν_{max} cm^{-1}): ν(C═O) 1598, ν(C═N) 1477. ^1H NMR (300 MHz, $CDCl_3$) δ 7.75 (m, 3H), 7.24–7.28 (d, 2H), 6.95–6.98 (d, 2H), 8.93 (s, 1H), 5.87 (dd, *J* = *J* = 17.9, 4.9 Hz, 1H), 3.79 (dd, *J* = 17.8, 11.6 Hz, 1H), 3.39 (dd, *J* = 11.7, 4.9 Hz, 1H). ^{13}C NMR ($CDCl_3$, 75 MHz): 160.09, 154.63, 142.77, 2132.11, 129.71, 128.14, 127.00, 125.36, 125.12, 54.57, 42.26, MS (*m/z*): 334.40 (M + 1), Calculated %: $C_{14}H_{11}BrN_2OS$: C 50.16; H 3.31; N 8.36. Found, %: C 50.20; H 3.48; N 8.38.

*2.2.11. 3-(3-bromophenyl)-5-(thiophen-2-yl)-4,5-dihydro-1H-pyrazole-1-carbaldehyde **(3k)***

Light green, Yield 79%. Mp: 160 °C. IR (neat, ν_{max} cm^{-1}): ν(C═O) 1655, ν(C═N) 1593. ^1H NMR ($CDCl_3$, 300 MHz): 7.56–7.65 (m, 4H), 7.21–7.43 (m, 1H), 6.93–6.96 (m, 2H), 8.95 (s, 1H), 5.85 (dd, *J* = 17.8, *J* = 4.6 Hz, 1H), 3.77 (dd, *J* = 17.8, 11.6 Hz, 1H), 3.36 (dd, *J* = 11.7, 4.6 Hz, 1H). ^{13}C NMR ($CDCl_3$, 75 MHz): 160.23, 155.81, 144.09, 132.33,

130.29, 129.14, 127.28, 125.89, 125.63, 124.55, 54.65, 42.28. MS (*m/z*): 334.40 (M + 1), Calculated %: $C_{14}H_{11}BrN_2OS$: C 50.16; H 3.31; N 8.36. Found, %: C 50.18; H 4.48; N 8.38.

2.2.12. 5-(4-(dimethylamino)phenyl)-3-(naphthalen-1-yl)-4,5-dihydro-1H-pyrazole-1-carbaldehyde **(3l)**

Light green, Yield 76%. Mp: 160 °C. IR (neat, ν_{max} cm^{-1}): ν(C═O) 1656, ν(C═N) 1596. ^1H NMR ($CDCl_3$, 300 MHz): 9.23–9.26 (d, 1H), 7.89– 7.94 (t, 2H), 7.45–7.69 (m, 4H), 7.18–7.25 (d, 2H), 6.67–6.70 (d, 2H), 9.07 (s, 1H), 5.47 (dd, J = 17.7, 4.6 Hz, 1H), 3.98 (dd, J = 17.8, 11.7 Hz,1H), 3.42 (dd, J = 17.7, 4.8 Hz, 1H), 2.94 (s, 6H). ^{13}C NMR ($CDCl_3$, 75.47 MHz): 160.33, 156.55, 150.31, 134.09, 131.40, 130.52, 128.79, 128.35, 127.82, 127.69, 126.83, 126.74, 126.48, 124.80, 112.78, 57.58, 45.12, 40.56. MS (*m/z*): 344.31 (M + 1), Calculated %: $C_{22}H_{21}N_3O$: C 76.94; H 6.16; N 12.24. Found, %: C 76.98; H 6.21; N 12.25.

2.3. In vitro cytotoxicity evaluation

Human lung cancer (**A549),** fibrosarcoma cell lines (**HT1080)** and human primary normal lung cells (**HFL-1)** were obtained from American type culture collection (ATCC, USA) and used in this study. Briefly, all these cell types were grown according to the standard culture conditions at 37 °C, with a 5% CO_2 in water-jacketed cell culture incubator. Respective cell culture media were used to culture these cells. **A549** cells were grown in DMEM media with 2 mM Glutamine, **HT1080** cells were grown in Eagle's Minimum Essential Medium (EMEM) as recommended, whereas **HFL-1** cells were also grown in F-12 K. All the media was supplemented with 10% FBS (Foetal bovine serum). For cell death analysis by the MTT method, 8000 cells were seeded in triplicates in a single 96 well plate. The plate was treated with increasing concentration made in the medium of 2, 4, 8, 16, 32, 64, and 128 μM of *N*-formyl pyrazoline derivatives and nocodazole dissolved in DMSO. The MTT assay was performed to check the effect of the test compounds on cell death after 24 h of treatment. After the treatment time was over, the media was discarded and gently each well was washed three times with PBS to remove the residual amount before performing the assay. As previously described, we used 10 μL of MTT reagent (Sigma, USA, Cat. No.11465007001) into each well having working stock concentration of 5 mg/ml. Following the addition of the MTT, the plates were incubated at 37 °C for 4 h. Once the incubation time was over, we used DMSO to remove crystals. Absorbance was measured at 570 nm using a hybrid multi-mode plate reader (BioTek, USA) with a microplate reader. We measured the percentage inhibition by the formula given below in Eq. (1):

$$\%\,\text{Inhibition} = 100 - \frac{\text{Mean OD of treated cells}}{\text{Mean OD of the vehicle control cells (negative control)}} \times 100 \quad (1)$$

We repeated the MTT assay three times with all the investigational compounds. IC_{50} values of the respective compounds were calculated using prism8 software (GraphPad) and expressed as a concentration (μM) of drugs.

2.4. Apoptosis studies

For quantitative apoptosis assay we used flow cytometry analysis on A549 cells. Cells were grown at 1.0×10^5 cells/ml and plated in a 24-well culture plate (Corning) for 24 h as mentioned above. Cells were treated with 4 μM of tested compounds **3b** and **3d** and incubated for another 24 h. For analysis, media was removed and cells were briefly washed with PBS followed by trypsinization protocol. Further, cells were suspended in PBS and stained with annex in V-FITC/PI as per the protocol provided by the supplier (Sigma, USA, Catalogue number: APOAF-20TST). Briefly, after addition of the reagents, cells were allowed incubated at room temperature for 30 min and analysed in PBS [37]. The assay has been performed with BD FACS Accuri (BD Biosciences, USA) and the data was analysed with FlowJo software (BD Biosciences, USA).

2.5. In silico molecular modelling and docking study

The crystal structure of topoisomerase II was retrieved from the protein data bank (PDB ID: 1ZXM) (www.rcsb.com) in PDB format. There were several missing residues in the crystal structure of topoisomerase II. The missing residues were added by the homology modelling method using modeller 9.10. Chemdraw software was used to draw the target drugs and to display and characterize their chemical structures. The procedure of molecular docking of the receptor topoisomerase II with pyrazoline derivatives (**3a–3l**) was carried out using the Autodock vina program 4.0 version of PyRx virtual screening tool [38]. The protein and target drugs were loaded in PyRx software and converting structure files into PDBQT format using the python script. The grid box was generated with a default grid spacing centered in the drug position and best confirmation was chosen for the evaluation of the lowest binding affinity. The docked protein-drug complex structures (including hydrogen bond, hydrophobic interaction and the bond lengths) were analyzed using the Discovery studio visualizer [39,40].

2.6. Relaxation assay of human topoisomerase II

Relaxation of negatively supercoiled plasmid DNA by human topoisomerase II (from nuclear extract of HeLa cells) was assayed in 20 μL of reaction buffer (10 mM Tris-HCl, pH 7.9, 150 mM NaCl, 0.1% BSA, 0.1 mM spermidine, 5% glycerol and 1 mM ATP) containing 250 ng of supercoiled pHOT1 plasmid DNA and 1 unit of enzyme. After incubation at 37 °C for 30 min, the reactions were terminated and analyzed by agarose gel electrophoresis. The ethidium bromide-stained gel was photographed over UV light for densitometry analysis. The percentage relaxation was determined by dividing the distance between the negatively supercoiled band (SC) and the weighted center of the partially relaxed band (PR) by the distance between the supercoiled band (SC) and the fully relaxed band (FR) to obtain percent relaxation = (SC-PR)/(SC-FR) (Reference Percent inhibition by different compounds was then calculated by subtracting percent relaxation in the presence of compounds from 100% relaxation obtained with enzyme only [41].

2.7. In silico ADMET assay

The *N*-formyl pyrozoline derivatives (**3a–3l**) were screened out based on the absorption, distribution, metabolism, excretion and toxicity properties. 2D structures of designed chemical compounds have been converted to canonical SMILES format and were used to compute the ADMET properties in the Molinspiration software. It plays a significant role in the drug design process and gives free access yet vigorous predictive models for physicochemical properties, pharmacokinetics and drug-likeness [34,42].

2.8. MD simulations

MD simulation is a useful tool to study the structure-function correlation in a protein [43–47]. The MD simulations were executed on topoisomerase II with its ligands **3b** and **3d** at 298 K by GROMACS 2018.2 [48]. The topology and force-field parameter files for **3b** and **3d** were externally obtained with the help of the PRODRG server [49]. The precise number of solvent and solute molecules were determined using a standard protocol [50–52]. To maintain neutrality, an adequate amount of Na^+ and Cl^- ions were added. The system was further minimized by increasing temperature from 0 to 298 K in the equilibration period. Equilibration was achieved by NVT and NPT ensembles at 100 ps. The

NVT ensemble includes a constant number of particles, volume and temperature, while NPT ensemble includes a constant number of particles, pressure and temperature. The particle-mesh Ewald method [53] was applied after the equilibration period, and finally, the production phases of 100 ns were performed at 298 K. The details of the MD methodology are explained in previous publications [52,54,55].

2.9. DNA binding studies

2.9.1. Absorption titration

Absorption titration has been performed to investigate the binding interaction of target analogs **3b** and **3d** with Ct-DNA. The absorption spectra were recorded in Tris-HCl/NaCl buffer in the range of 190–600 nm by varying the compounds concentration (0–60 μM) and keeping DNA concentration constant (40 μM). The absorbance ratio, A_{260}/A_{280} was 1.9:1 which indicate that the DNA was free from protein contamination. DNA concentration of stock solution was evaluated by taking its molar absorption coefficient (ε_{260}) 6600 l mol^{-1} cm^{-1} [56–60]. Test compounds were incubated for 10 min. and then absorption spectra was recorded.

Fig. 1. ^{1}H and ^{13}C NMR spectra of analogs 3b and 3d.

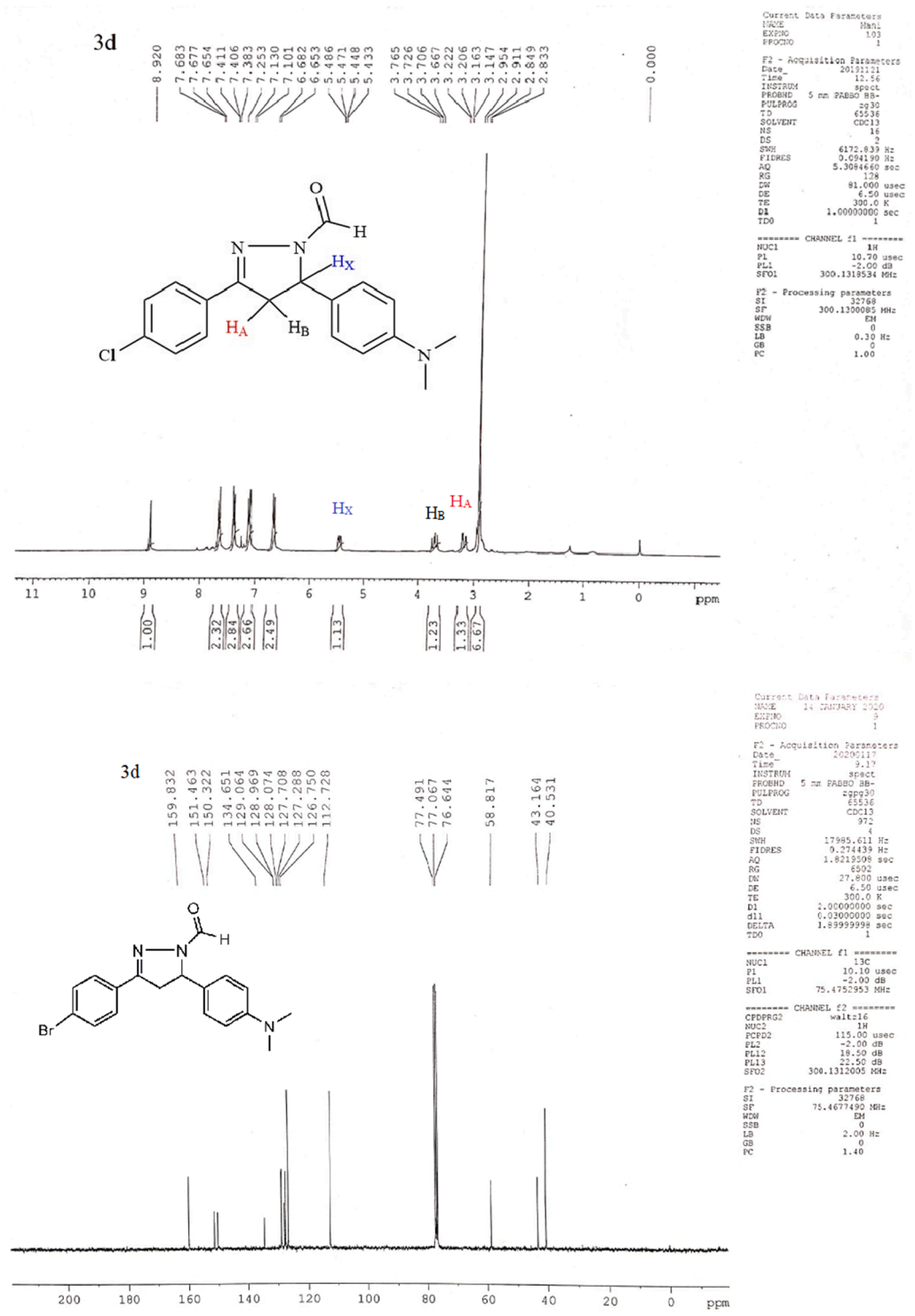

Fig. 1. (*continued*).

2.9.2. Fluorescence measurements

Fluorescence measurements were carried out to investigate the effect of compounds **3b** and **3d** on Ct-DNA. Fluorescence experiments were performed with the increasing concentration of Ct-DNA and fixing the compound concentration (40 μM). Samples were allowed to equilibrate for 30 min and after that fluorescence titration was done in tris–HCl/NaCl buffer in the range of 300–600 nm with an excitation wavelength of 320 nm for **3b** and 280 nm for **3d**. The slit widths were maintained at 10 nm for both emission and excitation [61–63].

2.9.3. Viscosity measurements

Viscosity measurements are considered as an effective and sensitive method to study the length change of helix. The Viscosity of Ct-DNA has been determined with and without test compound in 5 mM Tris– HCl/NaCl buffer (pH = 7.2). The Flow time of each sample was measured through the viscometer in triplicate and average value was used for the calculation. Viscosity measurements were carried out by gradually increasing the concentration of test compounds 0–60 μM and maintain the concentration of Ct-DNA constant (50 μM). The resulted data were ploted as $(\eta/\eta_0)^{1/3}$ versus [compound]/[DNA], where η is the viscosity

of Ct-DNA with compound and η_o is the viscosity of Ct-DNA without compound [19].

2.9.4. Circular dichroism

Circular dichroism (CD) is convenient and an excellent method to monitor the morphological changes that occur during DNA and drug interaction. These experiments were performed in 5 mM Tris-HCl/NaCl buffer in absence and presence of the compounds. All the experiments were performed in the range of 200–320 nm at room temperature [64]. Each sample was kept for 20 min at equilibrium before recording there spectrum and the spectra were repeated thrice to obtain the final average spectra at a scan rate 50 nm/min.

2.9.5. Electrochemical measurements

Cyclic voltammetry (CV) measurements were performed to get the information about the drug-DNA binding. A serially diluted 60 μL sample was purged on screen-printed electrode (SPE) to record the spectrum at a scan rate of 100 mVs^{-1} and voltage from −1 to +1 V. The measurements were performed in a solution of ferri/ferrocyanide (1:1) as redox couple. The further measurements of the lead compounds **3b** and **3d** were carried out with varying concentrations of Ct-DNA in tris–HCl/NaCl buffer. A film of test compounds was used as a working electrode and gold-coated copper was used as reference and counter electrode. Before the measurement, the pH value of the electrolytic solution was also controlled. The Entire analysis was accomplish at 25 °C with fixed potential scan rate of 50 mVs^{-1} in the potential align from +1.0 to −1.0 V at room temperature [65].

2.10. Antioxidant assay

2.10.1. DPPH radical scavenging activity

DPPH (2,2-diphenyl-1-picrylhydrazyl) scavenging capacity has been determined as per reported method [19,66]. To a solution of 3 ml of DPPH (0.1 mM) in ethanol, 1 ml of each test compounds (**3a–3l**) was added. The mixture solutions were incubated for 1 h and the decreasing in absorbance at 516 nm was recorded on a UV–visible spectrophotometer. Ethanol was used as blank and ascorbic acid was taken as a positive control. The entire experiment was performed in triplicate. The % inhibition antioxidant property was calculated by the following Eq. (2):

$$\%\,\text{Inhibition} = \frac{A_{\text{Control}} - A_{\text{Sample}}}{A_{\text{Control}}} \times 100 \quad (2)$$

where $A_{control}$ is absorbance of DPPH without compound and A_{sample} is absorbance of DPPH with compound.

2.10.2. Hydrogen peroxide scavenging activity

Hydrogen peroxide was also used for the estimation of the scavenging activity of test compounds using the reported method [67,68]. To the solution of 1.8 ml hydrogen peroxide (2 mM) in phosphate buffer was added 1 ml of test compounds in ethanol was added and then further diluted up to 4 ml with the phosphate buffer. All the samples were incubated for 10 min at 37 °C and absorbance was recorded at 230 nm on the UV–Vis spectrophotometer. Phosphate buffer was used as a blank and ascorbic acid was taken as a standard. The Ability of test samples to scavenge the hydrogen peroxide was measured by using the following Eq. (3):

$$\%\,\text{Inhibition} = \frac{A_B - A_T}{A_B} \times 100 \quad (3)$$

where A_B is absorbance of blank and A_T is absorbance of sample compounds.

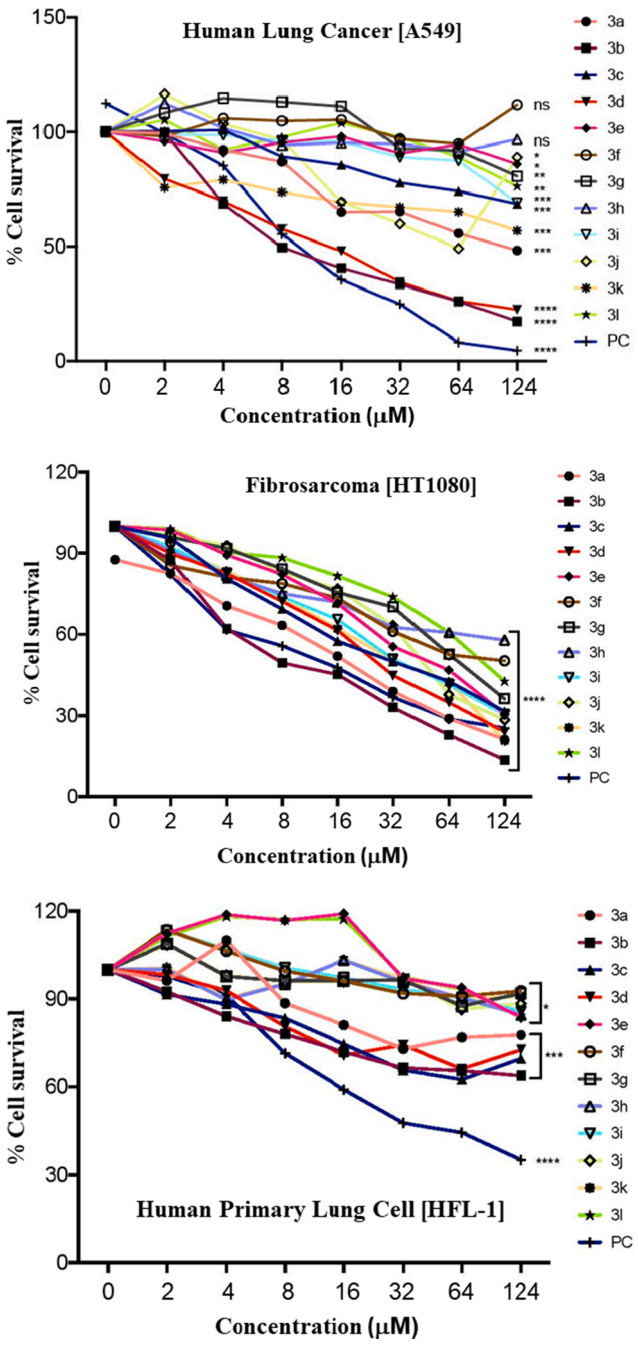

Fig. 2. Dose response % cell survival vs concentration of *N*-formyl pyrazoline derivatives **(3a–3l)**. Data is presented as Mean ± SEM. *indicates $P < 0.05$, **indicates $P < 0.01$, *indicates $P < 0.001$,****indicates $P < 0.0001$, and ns indicates non-significant. GraphPad prism was used to calculate statistical values by using non-parametric *t* test.

3. Results and discussion

3.1. Chemistry

The appropriate chalcones **(2a–2l)** were treated with hydrazine hydrate in the presence of formic acid by nucleophilic cycloaddition reaction followed the conventional heating method [10,41,69]. The formation of the *N*-formyl pyrazoline ring involves a Michael addition (1,4) of hydrazine on chalcone derivatives, followed by cyclization and dehydration. The synthesis of *N*-formyl pyrozoline derivatives **3a–3l** was followed in two steps with good yields of around 70–86%. The IR

Table 1
In vitro cytotoxicity and selectivity index (SI) of *N*-formyl pyrazoline derivatives **(3a–3l)** against human lung cancer cell lines (A549 and HT1080) and human primary normal lung cells (HFL-1) in terms of IC_{50} value in μM.

Compounds	A549	HT1080	HFL-1	Selectivity index	
				A549	HT1080
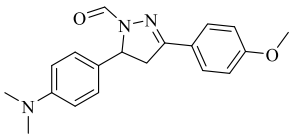	71.49 ± 8.37	26.03 ± 1.85	232.66 ± 7.35	3.2	8.9
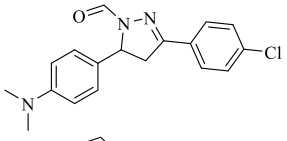	**12.47 ± 1.08**	**11.40 ± 0.66**	**116.47 ± 43.38**	9.3	10.2
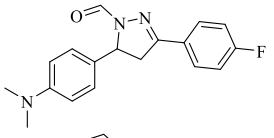	187.95 ± 33.31	31.4 ± 4.17	130.55 ± 47.23	0.6	4.1
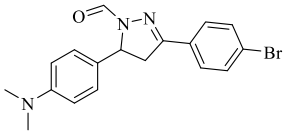	**14.46 ± 2.76**	**23.74 ± 13.30**	**152.36 ± 22.18**	10.5	6.4
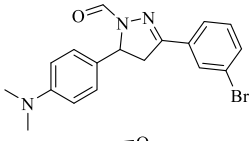	548.1 ± 124.022	46.99 ± 8.19	399.3 ± 33.89	0.7	8.4
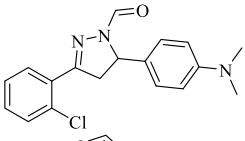	1032.55 ± 111.17	64.31 ± 2.83	531.36 ± 16.00	0.5	8.2
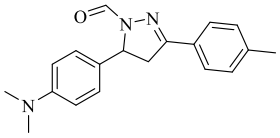	238.82 ± 60.43	66.89 ± 4.80	564.6 ± 29.72	2.3	8.4
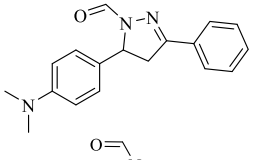	435.95 ± 225.02	83.13 ± 8.28	291.36 ± 82.14	0.6	3.5
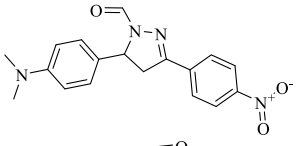	245.47 ± 80.49	35.39 ± 4.76	274.06 ± 14.91	1.1	7.7
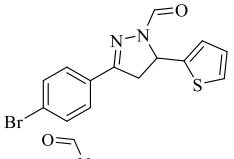	65.28 ± 15.30	48.07 ± 5.84	365.33 ± 39.31	5.5	7.5
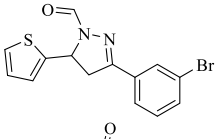	107.19 ± 70.62	31.56 ± 2.00	1163.43 ± 555.79	10.8	36.8
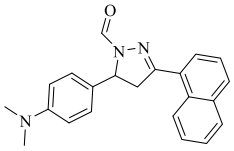	299.6 ± 98.00	90.51 ± 8.76	1066 ± 217.45	3.5	11.7
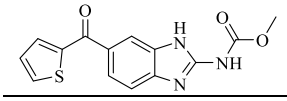	9.27 ± 0.60	14.49 ± 3.51	37.21 ± 13.76	4.0	2.5

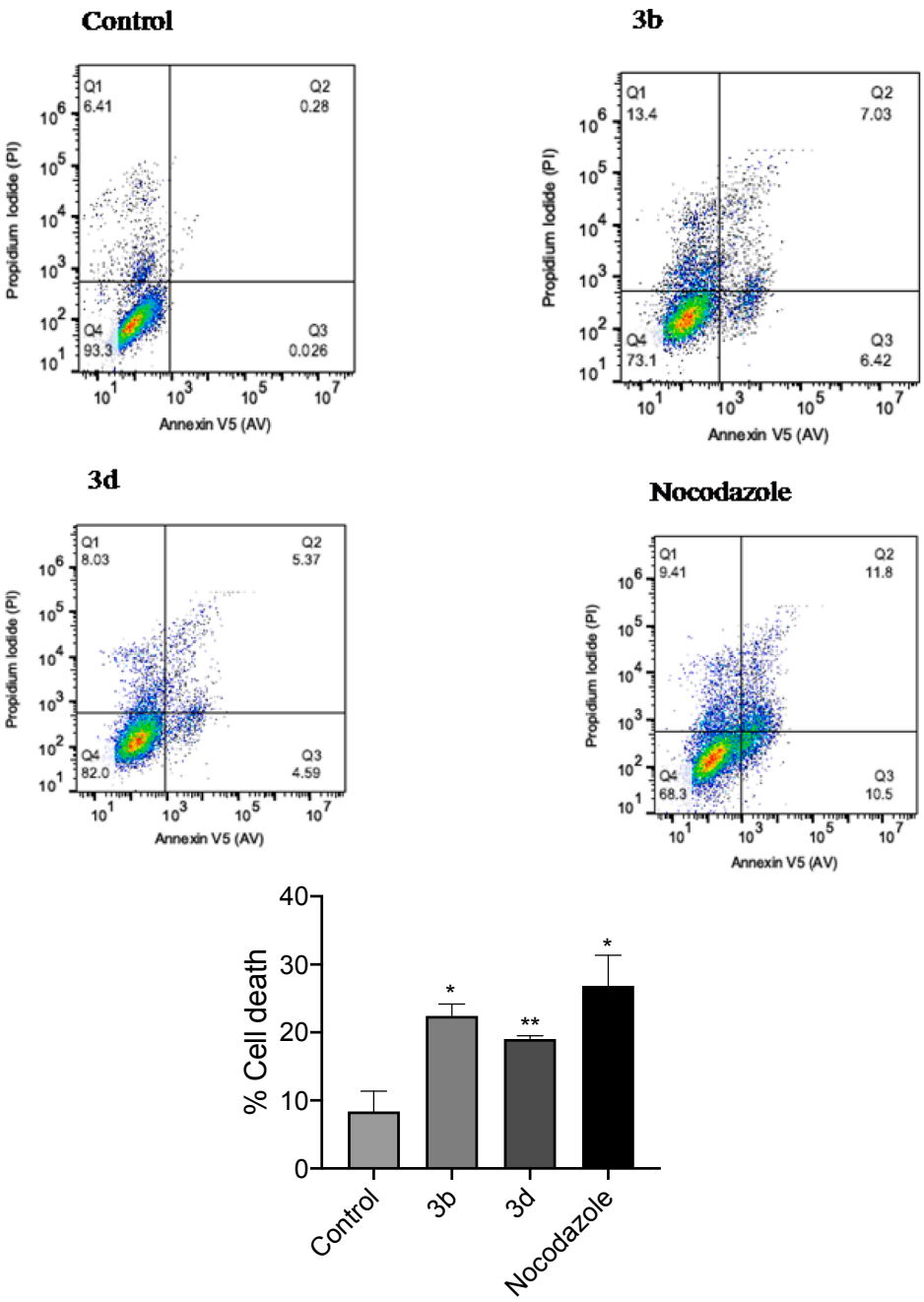

Fig. 3. Representative dot plots obtained after of apoptotic A549 cells after a 24 h treatment with 4 μM concentration of the analogs 3b, 3d, control and standard drug. The cells were harvested and labeled with Annexin-V(AV) and PI and then analyzed by flow cytometry. The histogram analysis of the respective drug treatments to show the statistical significance between various drugs treatments and control. The data is shown as Mean ± SEM. *indicates $P < 0.05$, and **indicates $P < 0.01$ with $n = 4$ in each sample. Non-parametric *t* test was used for the statistical comparisons.

spectra of the *N*-formyl pyrozoline derivatives **(3a–3l)** exhibits characteristics (C═O) and (C═N) absorption bands which appear at 1658–1579 and 1596–1460 cm^{-1} respectively (Fig. S2). The formation of pyrazoline ring in the target compounds was confirmed by revealed a typical ABX system, in which methylene proton resonated as a pair of doublets observed at 3.13–3.46 ppm (H_A), 3.66–3.99 ppm (H_B). The CH proton appeared as a doublet of doublets at 5.42–5.89 ppm (H_X) due to the vicinal coupling with the magnetically non-equivalents proton of the methylene group and a singlet of formyl proton at 8.91–9.23 ppm. The peaks of aromatic proton observed at 6.65–8.30 ppm. The main methylene signal in the ^{13}C NMR was observed at 42.22–59.41 ppm range. The signal observed between 159.83 and 161.48 ppm attributed to the (C═O) group, confirms the acetylation formation of the analogs (**3a-3l**) (Fig. 1 and Fig. S1). The mass spectra analyses were also supported by the structure of *N*-formyl pyrazoline derivatives **(3a–3l)** (Fig. S3).

3.2. Anticancer activity

In vitro cytotoxicity of all the synthesized *N*-formyl pyrozoline derivatives **(3a–3l)** was measured by MTT assay against human lung cancer (**A549),** fibrosarcoma (**HT1080)** cell lines and human primary normal lung cells (**HFL-1)** [70]. The calculated IC_{50} values were expressed as μM of the derivatives (**3a–3l**) (Fig. 2). Nocodazole was taken as a reference drug and the results in terms of IC_{50} values are given in Table 1. It is clear from the IC_{50} values that most of the pyrozoline derivatives showed moderate to good cytotoxicity against human lung cancer (**A549),** fibrosarcoma (**HT1080)** cell lines and very low toxicity towards human primary normal lung cells (**HFL-1).** The analogs **3a–3e** and **3i–3k** showed significant cytotoxicity as compared to standard drug nocodazole. The pyrazoline analogs **3a** and **3c** with OCH_3 and F groups in the *para*-substituted benzene ring showed an IC_{50} value of 26.03 ± 1.85 and 31.4 ± 4.17 μM against fibrosarcoma (**HT1080)** cell lines,

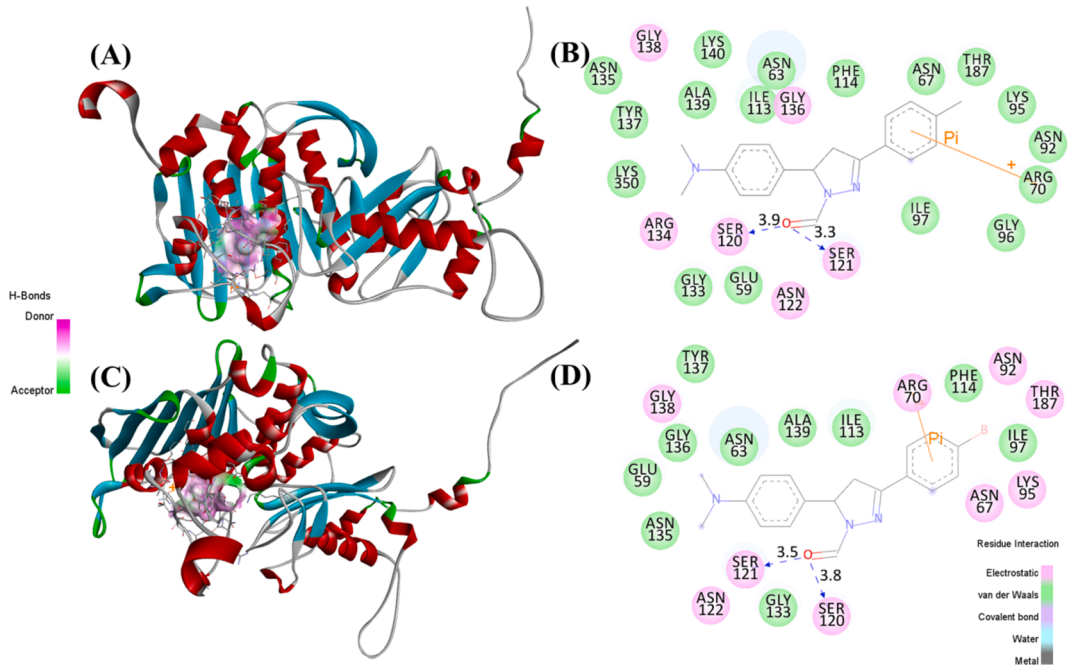

Fig. 4. Schematic representation of docked pose of (A and B) pyrazoline derivative 3b and (C and D) pyrazoline derivative 3d with topoisomerase II.

respectively. The analogs 3j and 3k containing thiophene ring with Br present in *para* and *meta* position of the benzene ring exhibited IC_{50} values of 48.07 ± 5.84 and 31.56 ± 2.00 μM against fibrosarcoma (**HT1080)** cell lines respectively. The compound 3i with NO_2 at the *para*-substituted benzene ring showed IC_{50} value of 35.39 ± 4.76 μM against fibrosarcoma (**HT1080)** cell lines. Compound **3e** with Br group at *meta*-substituted in parent analogue showed an IC_{50} value of 46.99 ± 8.19 μM against fibrosarcoma (**HT1080)** cell lines. The *N*-formyl pyrazoline analogs **3b** and **3d** exhibited excellent cytotoxicity with IC_{50} values of **12.47 ± 1.08** and **14.46 ± 2.76** μM against human lung cancer (**A549**) and **11.40 ± 0.66** and **23.74 ± 13.30** μM against fibrosarcoma (**HT1080**) cancer cell line as compared to standard drug nocodazole. Selectivity index (SI) data shown in Table 1 indicate that pyrazoline derivatives except 3b and 3d were non-selective for both the tested cancer cell lines as compared to the nocadazole.

3.3. Apoptosis study

To confirm the MTT findings of cell death, we used two lead compounds **3b** and **3d** for further evaluation by flow cytometry to get the quantitative estimate of the cell death. Based on the MTT assay results, we performed the assay on A549 cells. As shown in Fig. 3, robust cell death was elicited by the positive control drug (nocodazole), while very little cell death was observed in the control untreated cells. The cell death was measured as the percentage of positive cells in the three quadrants; Q1 reflecting the percentage of PI-positive cells, Q2 shows the percentage AV + PI positive cells, Q3 shows the percentage AV positive cells, and Q4 shows live cells. Increased signal in all the three quadrants (Q1-Q3) was observed, in the case of nocodazole treated cells with a concomitant decrease in the Q4 quadrant. On the contrary, a higher percentage of cells were seen in the Q4 quadrant in control cells, which confirm the validity of this assay for measuring cell death. Correspondingly, equal numbers of cells were used for analysis from the samples treated with the lead compounds 3b and 3d. Cells treated with these compounds showed increased cell death as measured by an increase in signal in the PI (Q1), Annexin V + PI (Q2), and Annexin V (Q3) quadrants. The overall cell death observed with **3b is 26.83** (**13.4 + 7.03 + 6.42**), and **3d** is **17.99** (**8.03 + 5.37 + 4.59**), as compared to

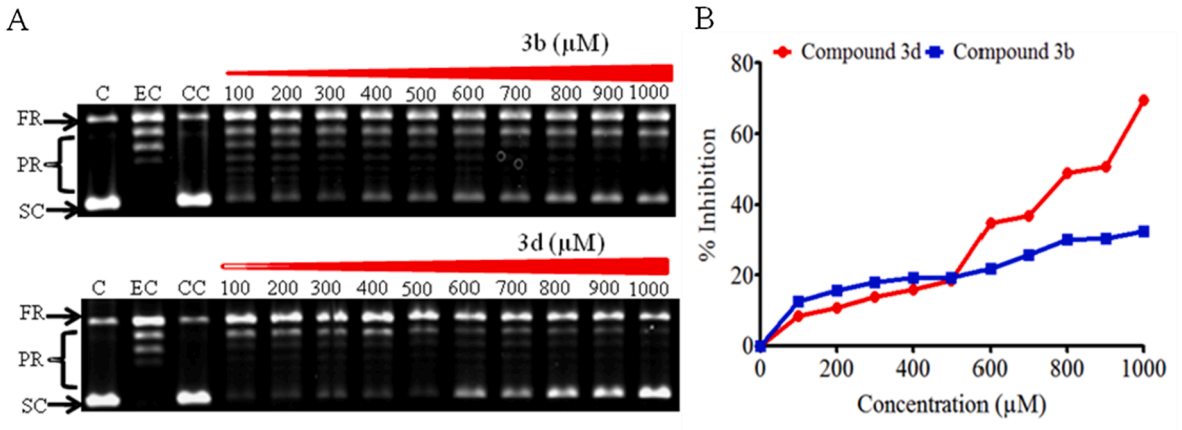

Fig. 5. Relaxation inhibition activity. A. Relaxation inhibition of HuTopoII by compounds 3b and 3d, C- pHOT1 plasmid only, EC- pHOT1 plasmid + enzyme, CC– pHOT1 plasmid + compound). FR- Fully Relaxed, PR- Partially Relaxed and SC- Supercolied plasmid. B. The quantification of percentage inhibition of relaxation of supercoiled plasmid by compounds 3b and 3d.

Table 2
Pharmacokinetics prediction of pyrazoline derivatives (**3a-3l**).

Compounds	MW <500	RB <10	Fraction Csp3	HBA HB 2–10	HBD HB <5	TPSA (<140 Å)	IlogP ≤5	GI absorption	QPlogPo/w (−2.0 to 6.5)	QP logkp (<5)	LV	MR ≤130	QPPCaco (nm/*sec*)<25 poor, >500 great)	QPPMDCK <25 poor, >500 great)	QPlogS <6
3a	323.40	5	0.26	3	0	45.14	2.7	High	2.63	−6.28	0	103.31	46.20	57.91	−3.42
3b	327.81	4	0.22	2	0	35.11	2.33	High	3.16	−5.84	0	101.83	50.29	92.40	−3.91
3c	311.36	4	0.22	3	0	35.11	2.42	High	2.93	−6.11	0	96.78	49.10	44.21	−3.36
3d	372.27	4	0.22	2	0	35.91	2.79	High	3.26	−6.06	0	104.52	44.31	11.27	−3.97
3e	372.27	4	0.22	2	0	35.91	2.82	High	3.27	−6.06	0	104.52	50.55	0.224	−3.97
3f	327.81	4	0.22	2	0	35.11	2.33	High	3.11	−5.84	0	101.83	50.29	12.48	−3.91
3g	307.40	4	0.26	2	0	35.91	2.59	High	2.96	−5.9	0	101.79	37.36	135.98	−3.63
3h	293.37	4	0.22	2	0	35.91	2.3	High	2.62	−6.07	0	96.82	36.56	151.97	−3.25
3i	338.37	4	0.22	4	0	81.73	2.07	High	1.89	−6.47	0	105.68	21.17	6.57	−4.04
3j	335.22	3	0.14	2	0	60.91	2.51	High	3.26	−6.13	0	88.19	43.98	12.05	−4.07
3k	335.22	3	0.14	2	0	60.91	2.5	High	3.26	−6.13	0	88.19	47.67	17.52	−4.07
3l	343.43	4	0.18	2	0	35.91	2.73	High	3.53	−5.49	0	114.33	36.8	20.75	−4.55
Nocodazole	301.32	5	0.07	4	2	112.32	1.26	High	2.25	−6.18	0	79.63	3.21	19.10	−3.61

Results indicate the abbreviate studied from SWISS ADMET where each abbreviate represent physicochemical properties for "drug likeliness" such as MW – Molecular weight; RB – Rotatable bond; HBA – Hydrogen bond acceptor; HBD – Hydrogen bond donor; TPSA – Topological polar surface area; IlogP– Logarithm of partition coefficient; GI – Gastrointestinal; QPlogPo/w – Predicted octanol/water partition coefficient; QPlogkp – Predicted skin permeability; LV – Lipinski violations; MR – Molar refractivity; QPPCaco – Apparent Caco-2 cell permeability; QPPMDCK – Apparent MDCK cell permeability; QPlogS – Predicted aqueous solubility.

6.716 in the **control** (**6.41 + 0.28 + 0.026**). These results thus suggest that both the lead compounds induce significant cell death which is comparable to the cell death induced by the nocodazole (Fig. 3). Overall, these results confirm the findings from MTT assay and suggest that these lead compounds may be potential anti-cancer drugs.

3.4. *In silico molecular modelling and docking study*

3D model of topoisomerase II was used for further docking and simulation studies. The discrete optimized protein energy (DOPE) score of model and template were found to be −42699.12 and −40736.66, respectively. This indicates the reliability of the predicted models which were subjected to further optimization and refinement. The molecular docking of pyrozoline derivatives (**3a–3l**) was carried out to find the best XP score (−6.2 to −8.4 kcal/mol). The docking was performed in the active pocket of topoisomerase II. The best pose was selected by analyzing the binding energy as well as superimposition of pre-existing ligands in the crystal of topoisomerase II to find the proper orientation of our docked ligands (Fig. 4). The binding energy of the compounds 3a, 3b, 3c, 3d, 3e, 3f, 3g, 3h, 3i, 3j, 3k, 3l and Nocodazole were found to be −8.1, −8.2, −7.5, −8.4, −6.7, −7.3, −7.1, −7.5, −6.5, −7.0, −6.2, −6.6 and −7.4 kcal/mol, respectively. Among all drugs, 3b and 3d showed higher binding affinity −8.1 and −8.4 kcal/mol respectively which indicate the good-quality results for topoisomerase II. This binding conformation of the topoisomerase II receptor in the active site is supposed to a reason for their significant inhibitory effect against pyrazoline derivatives.

3.5. *HuTopoII inhibitory activity*

Inhibitory activity of pyrazoline derivatives on HutopoII was examined via relaxation assay at varying concentrations 100–1000 μM. The target analogs 3b and 3d have shown inhibition of HutopoII relaxation activity at 1000 μM (Fig. 5). The pyrazoline derivatives other than 3b and 3d showed less HuTopoII inhibitory activity at higher concentration (Fig. S4). Gel densitometry analysis was performed to calculate the % inhibition of relaxation activity of HuTopoII for the synthesized compounds. Analogs 3b and 3d exhibited inhibition of relaxation upto 32% and ~70%, respectively at 1000 μM (Fig. 5). This finding further strengthens our in silico data, which showed compounds 3b and 3d have the strongest binding energy for topoisomerase II than other compounds. Our observation suggested that Cl and Br at para position could inhibit HuTopoII as observed in compounds 3b and 3d.

3.6. *ADMET prediction*

Lipinski's rule of five, also known as Rule of five (RO5), offers a valuable tool to assess the drug-likeness properties of a molecule [71,72]. According to this rule, the higher bioactivity score indicates a greater the chance of the specific compound will be active. It plays a significant role in drug design and development to the final success of drug candidates. All compounds following Lipinski's rule of five as well as bioactivity score for finding the more suitable result, including GPCR ligand, ion channel modulator, a kinase inhibitor, protease inhibitor and enzyme inhibitor as represented in Table 2. The lower value indicates better draggability. The range of various important parameters, like molecular weight, lied in range between 293 and 373, the value of total solvent accessible surface area (SASA) ranged 35–83 estimated number of hydrogen bonds donated (Donor H-B) by the solute to water molecules in an aqueous solutions was found 0, estimated number of hydrogen bonds accepted (accept H-B) by the solute to water molecules in an aqueous solutions ranged 2.00–4.00, predicted octanol/water partition coefficient (QPlogPo/w) ranged 1.89–3.53, predicted aqueous solubility (QPlogS), ranged −3.25 to −4.55, predicted number of rotatable bond (R.B) ranged 3–5, apparent Caco2 cell permeability (QPPCaco) ranged 21.17– 50.55 nm/*sec*, apparent MDCK cell

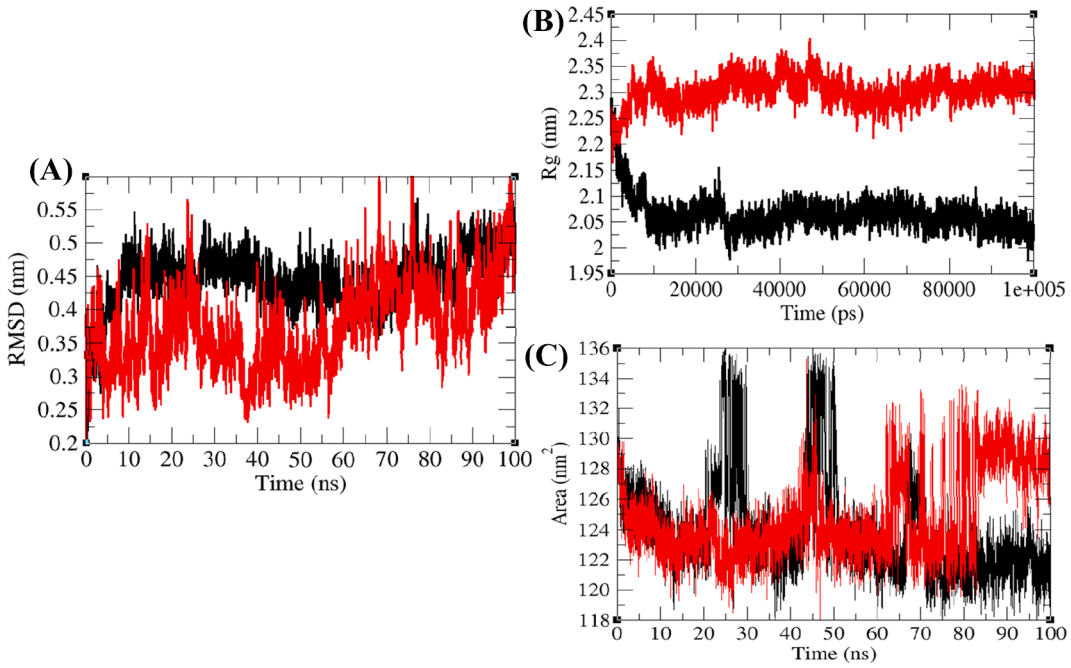

Fig. 6. Structural dynamics of topoisomerase II. **(A)** The plot of RMSD values, **(B)** the plot of Rg values and **(C)** the plot of SASA values of topoisomerase II with the ligands 3b (black) and 3d (red) at 100 ns MD simulations. (For interpretation of the references to colour in this figure legend, the reader is referred to the web version of this article.)

permeability (QPPMDCK) ranged 0.22–151.57 nm/*sec*, predicted skin permeability (QPlogKp) ranged −6.28 to −5.49, human GI absorption percentage is high, total polar surface area (PSA) ranged 35–83,IlogP ranged 2.3 to 2.82, molar refractivity ranged 88.19 to 114.19, fraction of sp3 hybridization ranged 0.14–0.22 and Lipinski violations were 0. These outcomes of ADMET studies were found to be within the acceptable range that following the drug-likeness properties of the pyrozoline derivatives, thus it suggests their potential as druggable molecules.

3.7. Structure deviation

To examine the impact of binding of analogs 3b and 3d in the structure of topoisomerase II, RMSD was calculated, which is a measure of protein conformation under particular conditions [51,53]. The average RMSD of topoisomerase II with 3b and 3d was found to be 0.44 nm and 0.31 nm, respectively. The binding of 3d leads to a decrease in RMSD values of topoisomerase II. It suggested that 3d binds more tightly than 3b to the active pocket of topoisomerase and stabilize the structure (Fig. 6A). This is also in line with the experimental and docking results. The average radius of gyration (R_g) values for topoisomerase II with 3b and 3d were found to be 2.06 nm and 2.30 nm, respectively (Fig. 6B). The R_g plot suggested that the compactness in the structure of topoisomerase II also changed due to the binding of these ligands. The binding of these ligands has different impacts on the structure of topoisomerase II. The solvent-accessible surface area (SASA) is describe as the surface area of a molecule that forms networks with the solvent [44,54]. The average SASA for backbone atoms of topoisomerase II with 3b and 3d were found to be 123.98 nm^2 and 124.82 nm^2, respectively (Fig. 6A). The SASA plot suggested that the binding of 3d leads to a slight increase in SASA values. This can be assumed as the core amino acid residues present in topoisomerase II were uncovered to solvent due to conformation change or denaturation.

3.8. DNA binding studies

3.8.1. Absorbance measurements

The Interaction ability of Ct-DNA with target compounds **3b** and **3d** has been studied to explore the binding mode of DNA by UV–visible spectroscopy. Hypochromic and hyperchromic are the two features that arise during absorption titrations of compounds. Hypochromic is due to the decrease in absorbance due to strong stacking interaction between the DNA base pairs and aromatic chromophore of the compounds, considered as a peculiar feature of intercalative mode of binding. However, hyperchromic is associated with the damage of the secondary structure of DNA and responsible for electrostatic or groove mode of binding [73,74]. The absorption spectra of the lead compound **3b** and **3d** in the presence and absence of Ct-DNA is shown in Fig. 7. From the results, hyperchromic was observed which confirmed that compounds bind to Ct-DNA through the electrostatic mode of binding. DNA binding constant (K_b) was determined to compare the DNA binding potency of the compoundsby using the Eq. (4):

$$[DNA]/(\varepsilon a - \varepsilon f) = [DNA]/\varepsilon b - \varepsilon f + 1/Kb(\varepsilon b - \varepsilon f) \quad (4)$$

Where ε_a refere to A_{obsd}/[Compound], however absorption extinction coefficient of free compound and in fully bound form, denoted as ε_f and ε_b, respectively. A plot of [DNA]/(ε_a–ε_f) versus [DNA] gave a slope 1/(ε_b–ε_f) and Y-intercept equal to 1/K_b(ε_b–ε_f) respectively. The Intrinsic binding constant (K_b) is slope to intercept ratio of the slope to intercept, found to be 2.0×10^4 and 3.0×10^3 M^{-1} for the compounds **3b** and **3d,** respectively.

3.8.2. Fluoremetric studies

Binding features of compounds **3b** and **3d** have been also explored with Ct-DNA by emission titrations as it provides a useful complement in support of the previous studies. Emission titrations of the compounds **3b** and **3d** were carried out in the presence of an increasing amount of Ct-DNA. It was observed that on each addition of Ct-DNA aliquot, the emission intensity increases significantly shown in Fig. 8. Results suggested that the quenching effect of the solvent molecule is prevented the hydrophobic environment of compounds inside the DNA helix. Transfer of photoelectron from the guanine base of DNA to excited states of the compounds is responsible for the quenching of emission of the compounds [75]. The emission data demonstrate that compounds **3b** and **3d** bind with DNA through the electrostatic mode of binding.

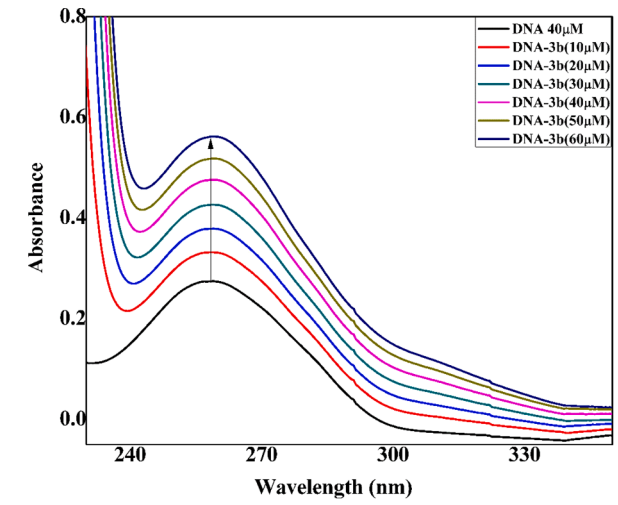

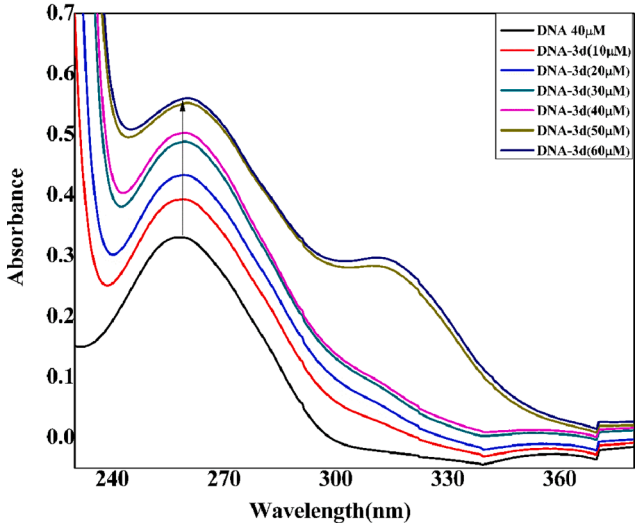

Fig. 7. Absorption spectra of Ct-DNA (40 μM) in the presence of increasing amounts of **3b** and **3d** (10–60 μM).

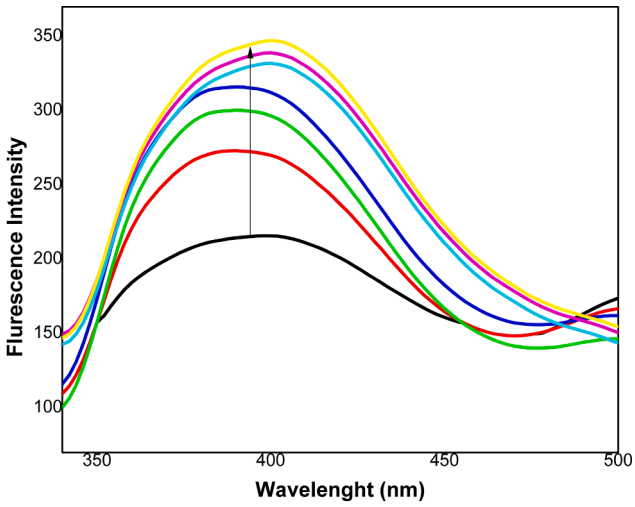

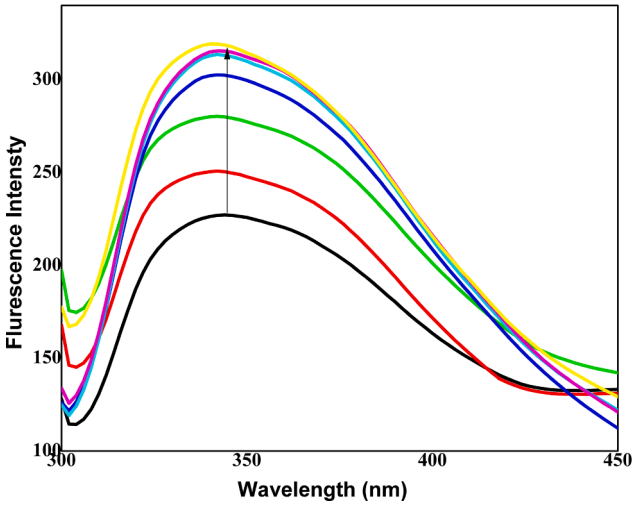

Fig. 8. Emission spectra of test compounds **3b** and **3d** (40 μM) in the presence of increasing [DNA] (0–60 μM).

3.8.3. *Viscosity measurements*

Compounds tend to adjust themselves between the DNA base pairs due to the separation of base pairs at the intercalation site which leads to increases in the viscosity of Ct-DNA, responsible for the classical intercalation mode of binding. Apart from this, in partial or non-classical intercalation mode, DNA helix bends or kinks to accommodate the compounds which also reduce the effective length Ct-DNA helix tends to decrease in viscosity. On addition of increasing amount of compounds (**3b** and **3d**) to a fixed amount of Ct-DNA, viscosity slightly increases (Fig. 9) [76]. The experimental results suggested that the compound can interact with Ct-DNA by electrostatic or groove mode of binding. These results are very similar with UV–Vis. and emission spectroscopic studies.

3.8.4. *Circular dichroism study*

CD spectroscopy is extensively used for monitoring the transformations that occurred in the secondary structure of DNA, proteins and polypeptides upon their interactions with ligand molecules. CD spectrum of DNA have been implement in the absence and presence of the target compounds (**3b** and **3d**) to investigate the conformational changes that occurred during drug-DNA interaction. Two characteristic peaks a positive band at 275 nm and a negative band at 245 nm shown by the native Ct-DNA, due to helicity of Ct-DNA and π-π base stacking, respectively [77]. Fig. 10 showed that the binding of compounds (**3b** and **3d**) to DNA did not have any remarkable effect on peak positions of 245 nm and 275 nm, only slightly decreased in intensity. Although, this little change in intensity at 245 nm and 275 nm may be attributed to certain conformational changes induced by binding of compounds (**3b** and **3d**) in which the B-conformation was still predominant. In general, electrostatic and groove binding have slight or no impact on DNA stand stacking and helicity although, intercalative binding influence deterministic outcome. This result explains the nature of the binding of target compounds (**3b** and **3d**) to Ct-DNA is non-intercalative. Moreover, the change induced by compound **3b** was more significant than **3d** which reveals that **3b** has a higher affinity for Ct- DNA.

3.8.5. *Electrochemical measurements*

Cyclic voltammetry (CV) experiments have also been performed for the support of DNA interaction studies. The binding of target compounds (**3b** and **3d**) with Ct-DNA has been inferred by the shift in peak potential in cyclic voltammogram [78]. Intercalation refers to the positive shift in peak potential however the electrostatic binding is due to the negative shift in peak potential. CV diagram of test compounds (**3b** and **3d**) with and without DNA is shown in Fig. 11. From the figure, it has been observed that after the addition of Ct-DNA to the compound, the peak potential is shifted in the positive direction and the peak current increased which may be due to the formation of the compound-DNA complex.

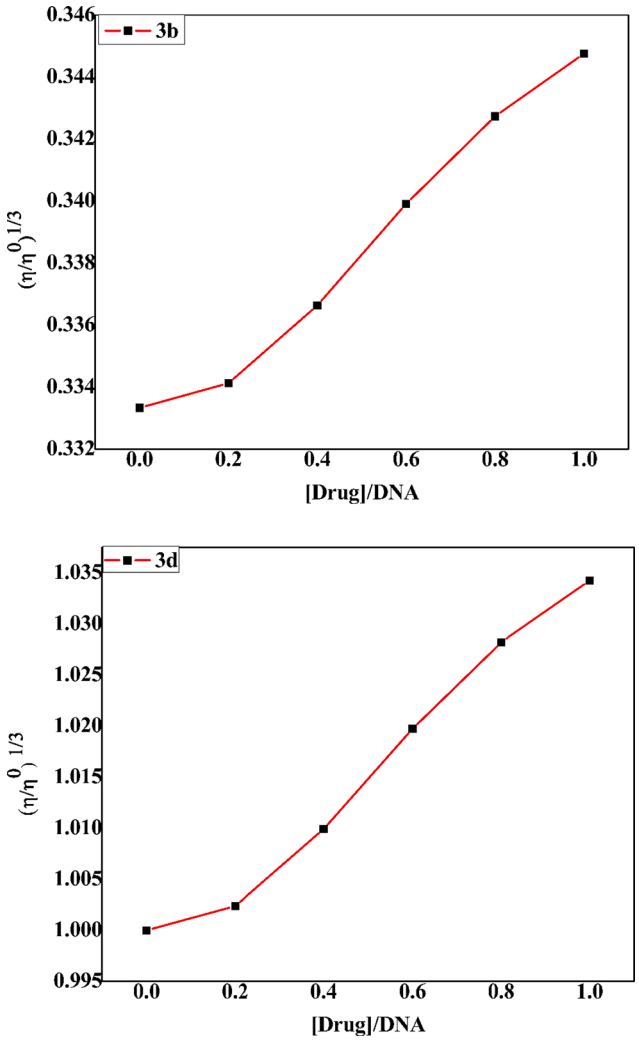

Fig. 9. Effect of increasing amounts of test compounds (10–50 μM) on the relative viscosity of DNA (50 μM).

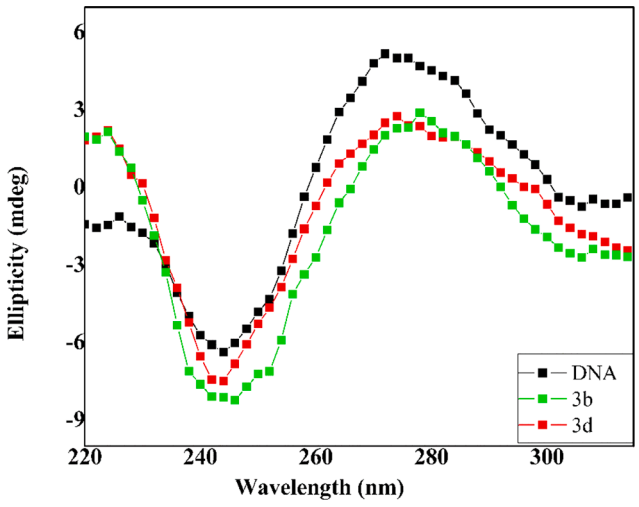

Fig. 10. Circular dichroism spectra of Ct-DNA (50 μM) in the absence and presence of test compounds **3b** and **3d** (50 μM).

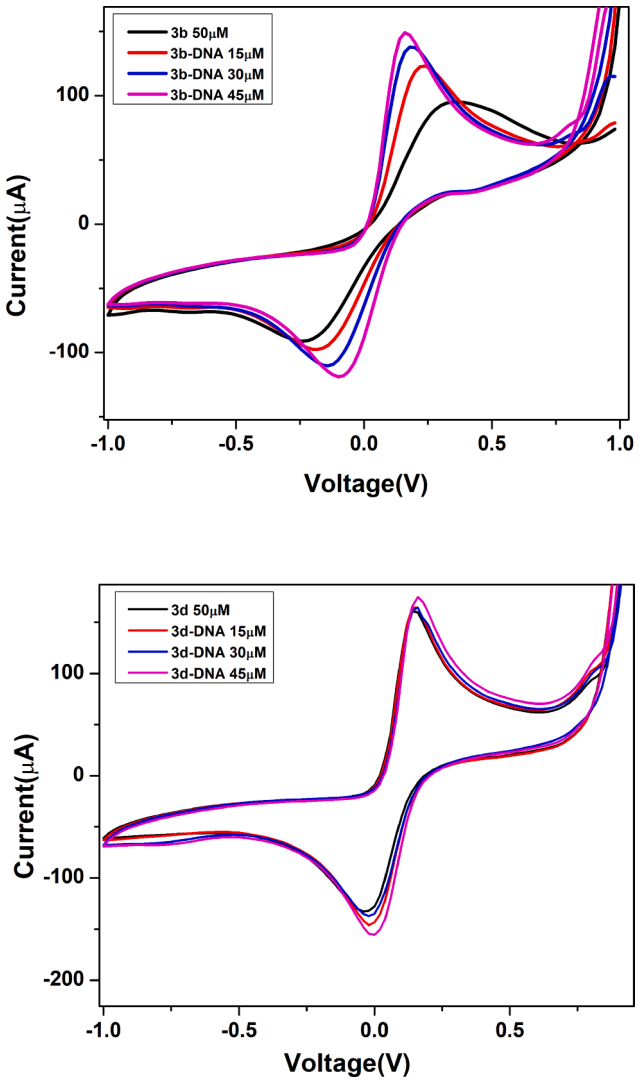

Fig. 11. Cyclic voltammogram of 5.0×10^{-5}M of test compounds **3b** and **3d** in 1 mM tris-buffer, pH 7.5 at 50 mV s^{-1} scan rate without DNA (black) and with DNA (red).

Table 3
% Antioxidant values with mean S.D. of pyrazoline derivatives **3a–3l** and ascorbic acid used as standard.

Compounds	DPPH (%)	H_2O_2 (%)
3a	69 ± 0.23	34 ± 0.67
3b	69 ± 0.34	24 ± 0.47
3c	73 ± 0.69	27 ± 0.37
3d	66 ± 0.54	20 ± 0.25
3e	66 ± 0.57	22 ± 0.34
3f	41 ± 0.13	33 ± 0.62
3g	74 ± 0.77	33 ± 0.65
3h	71 ± 0.21	33 ± 0.71
3i	70 ± 0.46	34 ± 0.59
3j	70 ± 0.67	34 ± 0.43
3k	70 ± 0.36	34 ± 0.23
3l	71 ± 0.68	33 ± 0.59
Ascorbic acid	89 ± 0.25	56 ± 0.62

3.9. Antioxidant assay

3.9.1. DPPH radical scavenging activity

DPPH is a free radical which can accept electron or hydrogen atom from the compound and become reduced. After the incubation of one

hour, the change in colour from violet to yellow was observed [19]. From the UV–visible spectrophotometer, it has been found that after the addition of test compounds absorbance was decreased at 516 nm. All the heterocyclic pyrazoline derivatives (**3a–3l**) exhibited significant antioxidant activity and results are shown in Table 3.

3.9.2. Hydrogen peroxide scavenging activity

For the evaluation of the antioxidant activity of the compounds (**3a–3l**), hydrogen peroxide assay is considered a very helpful method because it is highly reactive among all the oxygen- containing species [67]. The absorbance decreases after the addition of test compounds at 230 nm wavelength and compared with standard ascorbic acid (Table 3). All the results are DPPH free radical method.

4. Conclusion

In this article, we synthesized pyrazoline derivatives and then validated their structures by various spectroscopic techniques. Anticancer activity was evaluated against fibrosarcoma (**HT 1080**), human lung cancer (**A549**) cell lines and human primary normal lung cells (**HFL-1**). All the compounds showed moderate to good cytotoxicity and analogs **3b** and **3d** containing Cl and Br groups in the *para*-substituted benzene ring exhibit excellent cytotoxicity. The anticancer activity of the compounds was further validated by apoptosis and DNA binding studies. The binding strength of active compounds **3b** and **3d** with Ct-DNA was studied by UV–visible, fluorescence, viscocity, circular dichromism and cyclic voltametary techniques which showed an intercalation mode of binding. Molecular docking was used to evaluate the interaction of compounds, 3b and 3d with topoisomerase II, which showed their strongest binding energy with it. The computational results by molecular docking and MD simulation were in good agreement with the HuTopoII inhibitory activity observed experimentaly. The drug likeness properties of the compounds were further studied by computational method, ADMET assay, which strongly supported the experimental results. Overall the compounds showed excellent anticancer potential which could be further done by screening the compounds using different cell lines and *in vivo* studies.

Declaration of Competing Interest

The authors declare that they have no known competing financial interests or personal relationships that could have appeared to influence the work reported in this paper.

Acknowledgments

The authors thank to Centre for Instrumental Facility (CIF), Jamia Millia Islamia for providing necessary facility. MR also thanks to CSIR for financial assistance as NET JRF (File No: 09/466(0228)/2019).

Appendix A. Supplementary material

Supplementary data to this article can be found online at https://doi.org/10.1016/j.bioorg.2021.104665.

References

[1] V.R. Mishra, C.W. Ghanavatkar, S.N. Mali, H.K. Chaudhari, N. Sekar, Schiff base clubbed benzothiazole: synthesis, potent antimicrobial and MCF-7 anticancer activity, DNA cleavage and computational study, J. Biomol. Struct. Dyn. (2019) 1–14, https://doi.org/10.1080/07391102.2019.1621213.

[2] B. Sever, M.D. Altıntop, M.O. Radwan, A. Özdemir, M. Otsuka, M. Fujita, H.I. Ciftci, Design, synthesis and biological evaluation of a new series of thiazolyl-pyrazolines as dual EGFR and HER2 inhibitors, Eur. J. Med. Chem. 182 (2019) 111648, https://doi.org/10.1016/j.ejmech.2019.111648.

[3] A.F.C. Rengifo, N.M. Stefanes, J. Toigo, C. Mendes, D.F. Argenta, M.E.R. Dotto, M. C. Santos da Silva, R.J. Nunes, T. Caon, A.L. Parize, E. Minatti, PEO-chitosan nanofibers containing carboxymethyl-hexanoyl chitosan/dodecyl sulfate nanoparticles loaded with pyrazoline for skin cancer treatment, Eur. Polym. J. 119 (2019) 335–343, https://doi.org/10.1016/j.eurpolymj.2019.08.001.

[4] E. Bozkurt, H.I. Gul, Selective fluorometric "Turn-off" sensing for Hg^{2+} with pyrazoline compound and its application in real water sample analysis, Inorganica Chim. Acta. 502 (2020) 119288, https://doi.org/10.1016/j.ica.2019.119288.

[5] S. Chattopadhyay, Simplified treatment of electronic structures of the lowest singlet and triplet states of didehydropyrazines, J. Phys. Chem. A. 123 (28) (2019) 5980–5994, https://doi.org/10.1021/acs.jpca.9b03998.

[6] N.M. Stefanes, J. Toigo, M.F. Maioral, A.V. Jacques, L.D. Chiaradia-Delatorre, D. M. Perondi, A.A.B. Ribeiro, Á. Bigolin, I.M.S. Pirath, B.F. Duarte, R.J. Nunes, M. C. Santos-Silva, Synthesis of novel pyrazoline derivatives and the evaluation of death mechanisms involved in their antileukemic activity, Bioorg. Med. Chem. 27 (2) (2019) 375–382, https://doi.org/10.1016/j.bmc.2018.12.012.

[7] V. Nadaraj, S.T. Selvi, S. Mohan, T.D. Thangadurai, Microwave-assisted synthesis and pharmacological studies of novel 5-deazaalloxazine derivatives, Med. Chem. Res. 21 (10) (2012) 2911–2919, https://doi.org/10.1007/s00044-011-9811-1.

[8] A.V. Chate, A.A. Redlawar, G.M. Bondle, A.P. Sarkate, S.V. Tiwari, D.K. Lokwani, A new efficient domino approach for the synthesis of coumarin-pyrazolines as antimicrobial agents targeting bacterial alanine- ligase, New J. Chem. 43 (2019) 9002–9011, https://doi.org/10.1039/C9NJ00703B.

[9] S. Siliveri, N. Bashaboina, H.B. Vamaraju, S. Raj, Design, synthesis, molecular docking, admet studies and biological evaluation of pyrazoline incorporated 1, 2, 3-triazole benzene sulphonamides, Int. J. Pharm. Pharm. Sci. (2019) 6–15, https://doi.org/10.22159/ijpps.2019v11i6.32684.

[10] M.D. Nikam, P.S. Mahajan, M.G. Damale, J.N. Sangshetti, S.K. Dabhade, D. W. Shinde, C.H. Gill, Synthesis, molecular docking and biological evaluation of some novel tetrazolo[1,5-a]quinoline incorporated pyrazoline and isoxazoline derivatives, Med. Chem. Res. 24 (9) (2015) 3372–3386, https://doi.org/10.1007/s00044-015-1385-x.

[11] S.A. Khan, A.M. Asiri, N.S.M. Al-Ghamdi, M. Asad, M.E.M. Zayed, S.A.K. Elroby, F. M. Aqlan, M.Y. Wani, K. Sharma, Microwave assisted synthesis of chalcone and its polycyclic heterocyclic analogues as promising antibacterial agents: in vitro, in silico and DFT studies, J. Mol. Struct. 1190 (2019) 77–85, https://doi.org/10.1016/j.molstruc.2019.04.046.

[12] D. McPhee, Synthesis and characterization of new 3,5-dinaphthyl substituted 2-pyrazolines and study of their antimicrobial activity, Molecules. 11 (2006) 370, https://doi.org/10.3390/11050370.

[13] F.A. Ragab, Y.M. Nissan, E.M. Seif, A. Maher, R.K. Arafa, Synthesis and in vitro investigation of novel cytotoxic pyrimidine and pyrazolopyrimidne derivatives showing apoptotic effect, Bioorg. Chem. 96 (2020) 103621, https://doi.org/10.1016/j.bioorg.2020.103621.

[14] F. Hayat, A. Salahuddin, S. Umar, A. Azam, Synthesis, characterization, antiamoebic activity and cytotoxicity of novel series of pyrazoline derivatives bearing quinoline tail, Eur. J. Med. Chem. 45 (10) (2010) 4669–4675, https://doi.org/10.1016/j.ejmech.2010.07.028.

[15] M.D. Altıntop, A. Ozdemir, G. Turan-Zitouni, S. Ilgın, O. Atl, R. Demirel, Z. A. Kaplancıkl, A novel series of thiazolyl–pyrazoline derivatives: synthesis and evaluation of antifungal activity, cytotoxicity and genotoxicity, Eur. J. Med. Chem. 92 (2015) 342–352, https://doi.org/10.1016/j.ejmech.2014.12.055.

[16] X. Cai, S. Zhao, D. Cai, J. Zheng, Z. Zhu, D. Wei, Z. Zheng, H. Zhu, Y. Chen, Synthesis and evaluation of novel D-ring substituted steroidal pyrazolines as potential anti-inflammatory agents, Steroids 146 (2019) 70–78, https://doi.org/10.1016/j.steroids.2019.03.012.

[17] M.F. El Shehry, E.F. Ewies, E.M. Zayed, Synthesis of new pyrazole derivatives, their anti-inflammatory and analgesic activities, and molecular docking studies, Russ. J. Gen. Chem. 89 (3) (2019) 492–498, https://doi.org/10.1134/S1070363219030216.

[18] K. Zhou, L. Yu, Effects of extraction solvent on wheat bran antioxidant activity estimation, LWT - Food Sci. Technol. 37 (7) (2004) 717–721, https://doi.org/10.1016/j.lwt.2004.02.008.

[19] I.A. Ansari, F. Sama, M. Shahid, R. Rahisuddin, R. Arif, M. Khalid, Z.A. Siddiqi, Isolation of proton transfer complexes containing 4-picolinium as cation and pyridine-2,6-dicarboxylate complex as anion: crystallographic and spectral investigations, antioxidant activities and molecular docking studies, RSC Adv. 6 (14) (2016) 11088–11098, https://doi.org/10.1039/C5RA25939H.

[20] D.S. Raghuvanshi, N. Verma, S.V. Singh, S. Khare, A. Pal, A.S. Negi, Synthesis of thymol-based pyrazolines: an effort to perceive novel potent-antimalarials, Bioorg. Chem. 88 (2019) 102933, https://doi.org/10.1016/j.bioorg.2019.102933.

[21] A.K. Pandey, S. Sharma, M. Pandey, M.M. Alam, M. Shaquiquzzaman, M. Akhter, 4, 5-Dihydrooxazole-pyrazoline hybrids: synthesis and their evaluation as potential antimalarial agents, Eur. J. Med. Chem. 123 (2016) 476–486, https://doi.org/10.1016/j.ejmech.2016.07.055.

[22] C. Yamali, H.I. Gul, C. Kazaz, S. Levent, I. Gulcin, Synthesis, structure elucidation, and in vitro pharmacological evaluation of novel polyfluoro substituted pyrazoline type sulfonamides as multi-target agents for inhibition of acetylcholinesterase and carbonic anhydrase I and II enzymes, Bioorg. Chem. 96 (2020) 103627, https://doi.org/10.1016/j.bioorg.2020.103627.

[23] F. Anam, A. Abbas, K.M. Lo, Z.-u.-R. Zia-ur-Rehman, S. Hameed, M.M. Naseer, Homologous 1,3,5-triarylpyrazolines: synthesis, CH···π interactions guided self-assembly and effect of alkyloxy chain length on DNA binding properties, New J. Chem. 38 (11) (2014) 5617–5625, https://doi.org/10.1039/C4NJ00938J.

[24] B.S. Kitawat, M. Singh, Synthesis, characterization, antibacterial, antioxidant, DNA binding and SAR study of a novel pyrazine moiety bearing 2-pyrazoline derivatives, New J. Chem. 38 (9) (2014) 4290, https://doi.org/10.1039/C4NJ00594E.

[25] K.P. Thakor, M.V. Lunagariya, B.S. Bhatt, M.N. Patel, Synthesis, characterization and biological applications of some substituted pyrazoline based palladium (II) compounds, Appl. Organomet. Chem. 32 (11) (2018) e4523, https://doi.org/10.1002/aoc.v32.1110.1002/aoc.4523.
[26] J. Li, D. Li, Y. Han, S. Shuang, C. Dong, Synthesis of 1-phenyl-3-biphenyl-5-(N-ethylcarbazole-3-yl)-2-pyrazoline and its use as DNA probe, Spectrochim, Acta Part A Mol. Biomol. Spectrosc. 73 (2) (2009) 221–225, https://doi.org/10.1016/j.saa.2009.01.019.
[27] M.S. Muneera, J. Joseph, Design, synthesis, structural elucidation, pharmacological evaluation of metal complexes with pyrazoline derivatives, J. Photochem. Photobiol. B Biol. 163 (2016) 57–68, https://doi.org/10.1016/j.jphotobiol.2016.08.010.
[28] M.A. Diab, A.Z. El-Sonbati, S.M. Morgan, M.A. El-Mogazy, Polymer complexes. LXXI. Spectroscopic studies, thermal properties, DNA binding and antimicrobial activity of polymer complexes, Appl. Organomet. Chem. 32 (8) (2018) e4378, https://doi.org/10.1002/aoc.v32.810.1002/aoc.4378.
[29] N. Hijriani, L. Yusetyani, D. Hasmono, The effect of curcuma (Curcuma xanthorrizha roxb.) extract as an adjuvant of captopril therapy on cardiac histopathology of male mice (Mus musculus) with hypertension, J. Basic Clin. Physiol. Pharmacol. 30 (2020), https://doi.org/10.1515/jbcpp-2019-0280.
[30] R. Santosh, A. Prabhu, M.K. Selvam, P.M. Krishna, G.K. Nagaraja, P.D. Rekha, Design, synthesis, and pharmacology of some oxadiazole and hydroxypyrazoline hybrids bearing thiazoyl scaffold: antiproliferative activity, molecular docking and DNA binding studies, Heliyon 5 (2) (2019) e01255, https://doi.org/10.1016/j.heliyon.2019.e01255.
[31] D. Zhang, L. Gong, S. Ding, Y.e. Tian, C. Jia, D. Liu, M. Han, X. Cheng, D. Sun, P. Cai, Y.u. Tian, L.e. Yuan, W. Tu, J. Chen, A. Wu, Q.-N. Hu, FRCD: a comprehensive food risk component database with molecular scaffold, chemical diversity, toxicity, and biodegradability analysis, Food Chem. 318 (2020) 126470, https://doi.org/10.1016/j.foodchem.2020.126470.
[32] R.R. Varma, J.G. Pandya, F.U. Vaidya, C. Pathak, B.S. Bhatt, M.N. Patel, Biological activities of pyrazoline-indole based Re(I) carbonyls: DNA interaction, antibacterial, anticancer, ROS production, lipid peroxidation, in vivo and in vitro cytotoxicity studies, Chem. Biol. Interact. 330 (2020) 109231, https://doi.org/10.1016/j.cbi.2020.109231.
[33] Z.-G. Luo, Z.-Y. Liu, Z.-H. Yang, The synthesis and photoactivated cytotoxicity of novel 5-phenyl-3-(2,2′:5′,2″-terthien-5-yl)-4,5-dihydro-1H-pyrazolines, Chinese Chem. Lett. 25 (2) (2014) 333–336, https://doi.org/10.1016/j.cclet.2013.11.007.
[34] Y. Yang, C.-Y. Shi, J. Xie, J.-H. Dai, S.-L. He, Y. Tian, Identification of potential dipeptidyl peptidase (DPP)-IV inhibitors among moringa oleifera phytochemicals by virtual screening molecular docking analysis, ADME/T-based prediction, and in vitro analyses, Molecules. 25 (2020) 189, https://doi.org/10.3390/molecules25010189.
[35] S. Kuthyala, M. Hanumanthappa, S. Madan Kumar, S. Sheik, N. Gundibasappa Karikannar, A. Prabhu, Crystal, Hirshfeld, ADMET, drug-like and anticancer study of some newly synthesized imidazopyridine containing pyrazoline derivatives, J. Mol. Struct. 1197 (2019) 65–72, https://doi.org/10.1016/j.molstruc.2019.07.031.
[36] R. Shalaby, J.P. Petzer, A. Petzer, U.M. Ashraf, E. Atari, F. Alasmari, S. Kumarasamy, Y. Sari, A. Khalil, SAR and molecular mechanism studies of monoamine oxidase inhibition by selected chalcone analogs, J. Enzyme Inhib. Med. Chem. 34 (1) (2019) 863–876, https://doi.org/10.1080/14756366.2019.1593158.
[37] R.M. Hassan, W.H. Abd-Allah, A.M. Salman, A.A.-S. El-Azzouny, M.N. Aboul-Enein, Design, synthesis and anticancer evaluation of novel 1,3-benzodioxoles and 1,4-benzodioxines, Eur. J. Pharm. Sci. 139 (2019) 105045, https://doi.org/10.1016/j.ejps.2019.105045.
[38] S. Dallakyan, A.J. Olson, Small-molecule library screening by docking with PyRx, in (2015) 243–250, https://doi.org/10.1007/978-1-4939-2269-7_19.
[39] A.Z. El-Sonbati, M.A. Diab, Sh.M. Morgan, M.I. Abou-Dobara, A.A. El-Ghettany, Synthesis, characterization, theoretical and molecular docking studies of mixed-ligand complexes of Cu(II), Ni(II), Co(II), Mn(II), Cr(III), UO2(II) and Cd(II), J. Mol. Struct. 1200 (2020) 127065, https://doi.org/10.1016/j.molstruc.2019.127065.
[40] M.A. Diab, Gehad G. Mohamed, W.H. Mahmoud, A.Z. El-Sonbati, Sh.M. Morgan, S. Y. Abbas, Inner metal complexes of tetradentate Schiff base: synthesis, characterization, biological activity and molecular docking studies, Appl. Organomet. Chem. 33 (7) (2019), https://doi.org/10.1002/aoc.v33.710.1002/aoc.4945.
[41] R. Alam, D. Wahi, R. Singh, D. Sinha, V. Tandon, A. Grover, Rahisuddin, Rahisuddin, Design, synthesis, cytotoxicity, HuTopoIIα inhibitory activity and molecular docking studies of pyrazole derivatives as potential anticancer agents, Bioorg. Chem. 69 (2016) 77–90, https://doi.org/10.1016/j.bioorg.2016.10.001.
[42] A. Daina, O. Michielin, V. Zoete, SwissADME: a free web tool to evaluate pharmacokinetics, drug-likeness and medicinal chemistry friendliness of small molecules, Sci. Rep. 7 (2017) 42717, https://doi.org/10.1038/srep42717.
[43] S. Ali, F. Khan, T. Mohammad, D. Lan, M. Hassan, Y. Wang, Identification and evaluation of inhibitors of lipase from malassezia restricta using virtual high-throughput screening and molecular dynamics studies, Int. J. Mol. Sci. 20 (2019) 884, https://doi.org/10.3390/ijms20040884.
[44] A. Beg, F.I. Khan, K.A. Lobb, A. Islam, F. Ahmad, M.I. Hassan, High throughput screening, docking, and molecular dynamics studies to identify potential inhibitors of human calcium/calmodulin-dependent protein kinase IV, J. Biomol. Struct. Dyn. 37 (8) (2019) 2179–2192, https://doi.org/10.1080/07391102.2018.1479310.
[45] M. Gulzar, S.B. Syed, F.I. Khan, P. Khan, S. Ali, G.M. Hasan, P. Taneja, M.I. Hassan, Elucidation of interaction mechanism of ellagic acid to the integrin linked kinase, Int. J. Biol. Macromol. 122 (2019) 1297–1304, https://doi.org/10.1016/j.ijbiomac.2018.09.089.
[46] T. Mohammad, F.I. Khan, K.A. Lobb, A. Islam, F. Ahmad, M.I. Hassan, Identification and evaluation of bioactive natural products as potential inhibitors of human microtubule affinity-regulating kinase 4 (MARK4), J. Biomol. Struct. Dyn. 37 (7) (2019) 1813–1829, https://doi.org/10.1080/07391102.2018.1468282.
[47] F. Naz, F.I. Khan, T. Mohammad, P. Khan, S. Manzoor, G.M. Hasan, K.A. Lobb, S. Luqman, A. Islam, F. Ahmad, M.I. Hassan, Investigation of molecular mechanism of recognition between citral and MARK4: a newer therapeutic approach to attenuate cancer cell progression, Int. J. Biol. Macromol. 107 (2018) 2580–2589, https://doi.org/10.1016/j.ijbiomac.2017.10.143.
[48] D. Van Der Spoel, E. Lindahl, B. Hess, G. Groenhof, A.E. Mark, H.J.C. Berendsen, GROMACS: fast, flexible, and free, J. Comput. Chem. 26 (16) (2005) 1701–1718, https://doi.org/10.1002/(ISSN)1096-987X10.1002/jcc.v26:1610.1002/jcc.20291.
[49] A.W. Schuttelkopf, D.M.F. van Aalten, PRODRG : a tool for high-throughput crystallography of protein–ligand complexes, Acta Crystallogr. Sect. D Biol. Crystallogr. 60 (2004) 1355–1363, https://doi.org/10.1107/S0907444904011679.
[50] J.K. Carr, L.E. Buchanan, J.R. Schmidt, M.T. Zanni, J.L. Skinner, Structure and dynamics of urea/water mixtures investigated by vibrational spectroscopy and molecular dynamics simulation, J. Phys. Chem. B. 117 (42) (2013) 13291–13300, https://doi.org/10.1021/jp4037217.
[51] C. Camilloni, A. Guerini Rocco, I. Eberini, E. Gianazza, R.A. Broglia, G. Tiana, Urea and guanidinium chloride denature protein L in different ways in molecular dynamics simulations, Biophys. J. 94 (12) (2008) 4654–4661, https://doi.org/10.1529/biophysj.107.125799.
[52] S.B. Syed, F.I. Khan, S.H. Khan, S. Srivastava, G.M. Hasan, K.A. Lobb, A. Islam, F. Ahmad, M.I. Hassan, Mechanistic insights into the urea-induced denaturation of kinase domain of human integrin linked kinase, Int. J. Biol. Macromol. 111 (2018) 208–218, https://doi.org/10.1016/j.ijbiomac.2017.12.164.
[53] O.N. de Souza, R.L. Ornstein, Molecular dynamics simulations of a protein-protein dimer: particle-mesh ewald electrostatic model yields far superior results to standard cutoff model, J. Biomol. Struct. Dyn. 16 (6) (1999) 1205–1218, https://doi.org/10.1080/07391102.1999.10508328.
[54] S. Qausain, F.I. Khan, D. Lai, M.I. Hassan, M. Basheeruddin, N. Ahmed, M.K. A. Khan, Mechanistic insights into the urea-induced denaturation of a non-seleno thiol specific antioxidant human peroxiredoxin 6, Int. J. Biol. Macromol. 161 (2020) 1171–1180, https://doi.org/10.1016/j.ijbiomac.2020.05.168.
[55] M. Furkan, M.K. Siddiqi, S.M. Zakariya, F.I. Khan, M.I. Hassan, R.H. Khan, An In Vitro elucidation of the antiaggregatory potential of Diosminover thermally induced unfolding of hen egg white lysozyme; a preventive quest for lysozyme amyloidosis, Int. J. Biol. Macromol. 129 (2019) 1015–1023, https://doi.org/10.1016/j.ijbiomac.2019.02.107.
[56] S. Mathur, S. Tabassum, Template synthesis of novel carboxamide dinuclear copper (II) complex: spectral characterization and reactivity towards calf-thymus DNA, BioMetals 21 (3) (2008) 299–310, https://doi.org/10.1007/s10534-007-9119-2.
[57] Z. Asadi, N. Nasrollahi, H. Karbalaei-Heidari, V. Eigner, M. Dusek, N. Mobaraki, R. Pournejati, Investigation of the complex structure, comparative DNA-binding and DNA cleavage of two water-soluble mono-nuclear lanthanum(III) complexes and cytotoxic activity of chitosan-coated magnetic nanoparticles as drug delivery for the complexes, Spectrochim. Acta Part A Mol. Biomol. Spectrosc. 178 (2017) 125–135, https://doi.org/10.1016/j.saa.2017.01.037.
[58] M.N. Ahamad, M. Shahid, A. Ansari, M. Kumar, I.M. Khan, M. Ahmad, R. Arif, A combined experimental and theoretical approach to investigate the structure, magnetic properties and DNA binding affinity of a homodinuclear Cu (ii) complex, New J. Chem. 43 (2019) 7511–7519.
[59] A.Z. El-Sonbati, M.A. Diab, S.M. Morgan, A.M. Eldesoky, M.Z. Balboula, Polymer complexes. LXIX. Some divalent metal(II) polymer complexes of potentially bidentate monomer N-[4-(5-methyl-isoxazol-3-ylsulfamoyl)-phenyl]-acrylamide: synthesis, spectroscopic characterization, thermal properties, antimicrobial agents and DNA stud, Appl. Organomet. Chem. 32 (2018) e4207, https://doi.org/10.1002/aoc.4207.
[60] S.M. Morgan, A.Z. El-Sonbati, H.R. Eissa, Geometrical structures, thermal properties and spectroscopic studies of Schiff base complexes: correlation between ionic radius of metal complexes and DNA binding, J. Mol. Liq. 240 (2017) 752–776, https://doi.org/10.1016/j.molliq.2017.05.114.
[61] S. Rajalakshmi, T. Weyhermüller, M. Dinesh, B.U. Nair, Copper(II) complexes of terpyridine derivatives: a footstep towards development of antiproliferative agent for breast cancer, J. Inorg. Biochem. 117 (2012) 48–59, https://doi.org/10.1016/j.jinorgbio.2012.08.010.
[62] A.Z. El-Sonbati, M.A. Diab, S.M. Morgan, Thermal properties, antimicrobial activity and DNA binding of Ni(II) complexes of azo dye compounds, J. Mol. Liq. 225 (2017) 195–206, https://doi.org/10.1016/j.molliq.2016.11.047.
[63] Sh.M. Morgan, M.A. Diab, A.Z. El-Sonbati, Synthesis, spectroscopic, thermal properties, calf thymus DNA binding and quantum chemical studies of M(II) complexes, Appl. Organomet. Chem. 32 (5) (2018) e4281, https://doi.org/10.1002/aoc.v32.510.1002/aoc.4281.
[64] P. Xi, Z. Xu, X. Liu, F. Cheng, Z. Zeng, Synthesis, characterization and DNA-binding studies of 1-cyclohexyl-3-tosylurea and its Ni(II), and Cd(II) complexes, spectrochim, Acta Part A Mol. Biomol. Spectrosc. 71 (2) (2008) 523–528, https://doi.org/10.1016/j.saa.2008.01.005.
[65] M. Pešić, J. Bugarinović, A. Minić, S.B. Novaković, G.A. Bogdanović, A. Todosijević, D. Stevanović, I. Damljanović, Electrochemical characterization and estimation of DNA-binding capacity of a series of novel ferrocene derivatives, Bioelectrochemistry 132 (2020) 107412, https://doi.org/10.1016/j.bioelechem.2019.107412.

[66] S. Thalamuthu, B. Annaraj, M.A. Neelakantan, A systematic investigation on biological activities of a novel double zwitterionic Schiff base Cu(II) complex, Spectrochim. Acta - Part A Mol. Biomol. Spectrosc. 118 (2014) 120–129, https://doi.org/10.1016/j.saa.2013.08.065.

[67] M. Iranifam, H.A.J. Al Lawati, Monitoring the antioxidant capacity in honey and fruit juices using a microfluidic device with a $NaHCO_3$-H_2O_2-Co^{2+} chemiluminescence reaction, Food Chem. 297 (2019) 124930, https://doi.org/10.1016/j.foodchem.2019.05.204.

[68] J. Yang, X. Song, Y. Feng, N. Liu, Z. Fu, J. Wu, T. Li, H. Chen, J. Chen, C. Chen, L. Yang, Natural ingredients-derived antioxidants attenuate H_2O_2-induced oxidative stress and have chondroprotective effects on human osteoarthritic chondrocytes via Keap1/Nrf2 pathway, Free Radic. Biol. Med. 152 (2020) 854–864, https://doi.org/10.1016/j.freeradbiomed.2020.01.185.

[69] R. Alam, M.A. Alam, A.K. Panda, Rahisuddin, Design, Synthesis, and Cytotoxicity Evaluation3-(5-(3-(aryl)-1-phenyl-1H-pyrazol-4-yl)-1-phenyl-4,5-dihydro-1H-pyrazol-3-yl)pyridine5-(3-(aryl)-1-phenyl-1H-pyrazol-4-yl)-3-(pyridin-3-yl)-4,5-dihydropyrazole-1-carbaldehyde Derivatives as Potential, J. Heterocycl. Chem. 54 (2017) 1812–1821, https://doi.org/10.1002/jhet.2768.

[70] K. Chen, Y.-L. Zhang, J. Fan, X. Ma, Y.-J. Qin, H.-L. Zhu, Novel nicotinoyl pyrazoline derivates bearing N-methyl indole moiety as antitumor agents: design, synthesis and evaluation, Eur. J. Med. Chem. 156 (2018) 722–737, https://doi.org/10.1016/j.ejmech.2018.07.044.

[71] F. Curreli, D.S. Belov, Y. Do Kwon, R. Ramesh, A.M. Furimsky, K. O'Loughlin, P. C. Byrge, L.V. Iyer, J.C. Mirsalis, A.V. Kurkin, A. Altieri, A.K. Debnath, Structure-based lead optimization to improve antiviral potency and ADMET properties of phenyl-1H-pyrrole-carboxamide entry inhibitors targeted to HIV-1 gp120, Eur. J. Med. Chem. 154 (2018) 367–391, https://doi.org/10.1016/j.ejmech.2018.04.062.

[72] P. Tripathi, S. Ghosh, S.N. Talapatra, Bioavailability prediction of phytochemicals present in Calotropis procera (Aiton) R. Br. by using Swiss-ADME tool, WSN. 131 (2019) 147–163.

[73] S. Pedatella, C. Cerchia, M. Manfra, A. Cioce, A. Bolognese, A. Lavecchia, Antitumor agents 7. Synthesis, antiproliferative activity and molecular modeling of new l-lysine-conjugated pyridophenoxazinones as potent DNA-binding ligands and topoisomerase IIα inhibitors, Eur. J. Med. Chem. 187 (2020) 111960, https://doi.org/10.1016/j.ejmech.2019.111960.

[74] A. Meščić Macan, N. Perin, S. Jakopec, M. Mioč, M.R. Stojković, M. Kralj, M. Hranjec, S. Raić-Malić, Synthesis, antiproliferative activity and DNA/RNA-binding properties of mono- and bis-(1,2,3-triazolyl)-appended benzimidazo[1,2-a] quinoline derivatives, Eur. J. Med. Chem. 185 (2020) 111845, https://doi.org/10.1016/j.ejmech.2019.111845.

[75] R. Arif, M. Rana, S. Yasmeen, Amaduddin, M.S. Khan, M. Abid, M.S. Khan, Rahisuddin, Facile synthesis of chalcone derivatives as antibacterial agents: synthesis, DNA binding, molecular docking, DFT and antioxidant studies, J. Mol. Struct. 1208 (2020) 127905, https://doi.org/10.1016/j.molstruc.2020.127905.

[76] J. Kovvuri, B. Nagaraju, V.L. Nayak, R. Akunuri, M.P.N. Rao, A. Ajitha, N. Nagesh, A. Kamal, Design, synthesis and biological evaluation of new β-carboline-bisindole compounds as DNA binding, photocleavage agents and topoisomerase I inhibitors, Eur. J. Med. Chem. 143 (2018) 1563–1577, https://doi.org/10.1016/j.ejmech.2017.10.054.

[77] S. Yasmeen, Riyazuddeen, G. Rabbani, Rabbani, Calorimetric and spectroscopic binding studies of amoxicillin with human serum albumin, J. Therm. Anal. Calorim. 127 (2) (2017) 1445–1455, https://doi.org/10.1007/s10973-016-5555-y.

[78] T. Sarwar, M.A. Husain, S.U. Rehman, H.M. Ishqi, M. Tabish, Multi-spectroscopic and molecular modelling studies on the interaction of esculetin with calf thymus DNA, Mol. Biosyst. 11 (2) (2015) 522–531, https://doi.org/10.1039/C4MB00636D.